

# Higher-order Graph Convolutional Network with Flower-Petals Laplacians on Simplicial Complexes

Yiming Huang<sup>1,2,\*</sup>, Yujie Zeng<sup>1,2,\*</sup>, Qiang Wu<sup>1,†</sup>, Linyuan Lü<sup>3,1,2,†</sup>

<sup>1</sup>Institute of Fundamental and Frontier Sciences,

University of Electronic Science and Technology of China, Chengdu, 611731, China

<sup>2</sup>Yangtze Delta Region Institute (Huzhou), University of Electronic Science and Technology of China, Huzhou 313001, China

<sup>3</sup>School of Cyber Science and Technology, University of Science and Technology of China, Hefei 230026, China  
{yiming\_huang, yujie\_zeng}@std.uestc.edu.cn, {qiang.wu, linyuan.lv}@uestc.edu.cn

## Abstract

Despite the recent successes of vanilla Graph Neural Networks (GNNs) on many tasks, their foundation on pairwise interaction networks inherently limits their capacity to discern latent higher-order interactions in complex systems. To bridge this capability gap, we propose a novel approach exploiting the rich mathematical theory of simplicial complexes (SCs) - a robust tool for modeling higher-order interactions. Current SC-based GNNs are burdened by high complexity and rigidity, and quantifying higher-order interaction strengths remains challenging. Innovatively, we present a higher-order Flower-Petals (FP) model, incorporating FP Laplacians into SCs. Further, we introduce a Higher-order Graph Convolutional Network (HiGCN) grounded in FP Laplacians, capable of discerning intrinsic features across varying topological scales. By employing learnable graph filters, a parameter group within each FP Laplacian domain, we can identify diverse patterns where the filters' weights serve as a quantifiable measure of higher-order interaction strengths. The theoretical underpinnings of HiGCN's advanced expressiveness are rigorously demonstrated. Additionally, our empirical investigations reveal that the proposed model accomplishes state-of-the-art (SOTA) performance on a range of graph tasks and provides a scalable and flexible solution to explore higher-order interactions in graphs.

## 1 Introduction

Graphs are ubiquitous in representing irregular relations in various scenarios. However, they are inherently constrained to modeling pairwise interactions exclusively (Battiston et al. 2020). Many empirical systems display group interactions, going beyond pairwise connections, such as social systems (Centola 2010), neuronal networks (Ganmor, Segev, and Schneidman 2011), and ecological networks (Grilli et al. 2017). However, such higher-order interactions can hardly be modeled or approximated in pairwise graphs. In addition, it is still elusive how to quantify the strength of higher-order interaction, although many studies have demonstrated its existence (Battiston et al. 2021).

Graph neural networks (GNNs) can exploit the features and topology of graphs simultaneously, thereby triggering a wide-spreading research interest and endeavor in various

graph learning tasks such as recommender systems (Wu et al. 2022) and new drug discovery (Zitnik, Agrawal, and Leskovec 2018). In particular, spectral GNNs have been widely recognized for their rigorous mathematical theory. Nevertheless, pairwise-graph-based GNNs fail to capture latent higher-order interactions prevalent in empirical systems, and their expressive power was proved to be upper bounded by Weisfeiler-Lehman (WL) test (Xu et al. 2019).

Simplicial complexes (SCs) and hypergraphs have been developed to study higher-order interactions that extend beyond the conventional pairwise descriptors (Battiston et al. 2020). Hypergraph learning has made fruitful achievements (Gao et al. 2022), but it typically ignores relations within the hyperedges, and the construction of hypergraphs is often under-optimized. The simplicial description is another potent tool with elegant mathematical theories to draw from, and it paves a middle ground between graphs and hypergraphs. It has been found that SCs play a vital role in the social contagion (Battiston et al. 2021), synchronization (Gambuzza et al. 2021), brain network analysis (Sizemore et al. 2018), etc.

Deep learning facilitated simplicial complex theory is a fresh perspective and promising research field. Several simplicial GNNs have been proposed by simply replacing the graph Laplacian with the Hodge Laplacian (Schaub et al. 2020). A simplicial WL test is proposed along with its neural version MPSN (Bodnar et al. 2021) based on the adjacency relations that Hodge theory defines. MPSN is proved to be more powerful than vanilla GNNs under ideal conditions, implying the potential of extending graph representation learning to SCs.

In summary, pairwise GNNs fail to capture latent group interactions prevalent in complex systems, and the expressive power of such models was proved to be upper bounded by WL-test. As an emerging and promising research field, simplicial GNNs have initially shown their potential to outperform pairwise GNNs. However, existing models are limited by their high complexity and low flexibility.

In this paper, we introduce a novel higher-order flower-petals (FP) representation based on two-step random walk dynamics between the flower core and petals. This representation enables us to incorporate interactions among simplices of various orders into graph learning. Higher-order

\*These authors contributed equally.

†Corresponding author.

graph convolutional network (HiGCN) is then proposed by employing learnable and tailored convolution filters (group of parameters) in different FP Laplacian domains. The learnable filters can learn arbitrary shapes and deal with high and low-frequency parts of the simplicial signals adaptively. Hence, the proposed HiGCN model can learn the simplex patterns of disparate classes and higher-order structures simultaneously. Moreover, the filters’ weights in different orders can quantify the higher-order interaction strength, contributing to a deeper understanding of higher-order mechanisms in complex systems. We also interpret HiGCN from the message-passing perspective and theoretically demonstrate its superior expressive power. Numerical experiments on various graph tasks further pinpoint that the proposed model has outperformed state-of-the-art (SOTA) methods.

**Main Contributions.** To summarise, we construct an innovative higher-order flower-petals (FP) model and FP Laplacians from the random walk dynamics between the flower core and petals to capture interactions among simplices of different orders. Then, we propose a higher-order graph convolutional network (HiGCN) framework based on our FP Laplacians for graph representation learning. A data-driven strategy is employed to demonstrate the existence of higher-order interactions and to quantify the interaction strength. Finally, we theoretically demonstrate HiGCN’s superior expressive power along with significant performance gains in various empirical experiments. In general, our work is an important step toward studying the higher-order mechanism in complex networks.

## 2 Related work

In this section, we briefly review related work on vanilla spectral GNNs and higher-order GNNs.

**Spectral GNNs.** Spectral GNNs are based on the graph Fourier transform (Shuman et al. 2013), which employs the graph Laplacian eigenbasis as an analogy of the Fourier transform. Bruna et al. (2014) developed spectral graph convolutional networks based on the spectrum of the graph Laplacian. ChebNet (Defferrard, Bresson, and Vandergheynst 2016) employs Chebyshev polynomials to replace the convolutional core, while GCN (Kipf and Welling 2017) uses a first-order approximation of the convolution operator. By considering the relationship between GCN and PageRank, APPNP (Gasteiger, Bojchevski, and Günnemann 2019) is proposed via personalized PageRank. GPRGNN (Chien et al. 2020) leverages a learnable graph filter, exhibiting superiority in heterogeneous graph learning. The filter forms of some spectral GNNs are summarized in Table 1.

**Higher-order GNNs.** The crude simplification of complex interaction into pairwise will inevitably result in information loss. Higher-order GNNs, as extensions of vanilla GNNs, can be classified into different types according to their application scenarios, and spectral-based simplicial GNNs are in the limelight of this paper. The Hodge theory (Hatcher 2002) enables us to describe diffusion across simplices conveniently. Several simplicial GNNs (Ebli, Defferrard, and Spreemann 2020; Roddenberry, Glaze, and Segarra

2021) simply replace the graph Laplacian with the Hodge  $p$ -Laplacian. SCNN (Yang, Isufi, and Leus 2022) employs flexible simplicial filters to process edge signals from lower and upper simplicial neighbors, respectively. BScNet (Chen, Gel, and Poor 2022) is introduced by replacing the graph Laplacian with the block Hodge Laplacian. Nevertheless, the Hodge theory is inherently constrained to modeling interactions between simplices within one order difference. As for spatial models, SGAT (Lee, Ji, and Tay 2022) constructs SCs from heterogeneous graphs and leverages upper adjacencies to pass messages between simplices. MPSN (Bodnar et al. 2021) is designed based on the simplicial WL-test with four types of adjacency relations. Generally, most simplicial GNNs can only leverage information from specific simplicial orders, missing the inherent advantages of SCs. Besides, it is computationally expensive to find all simplices (Bomze et al. 1999) and unnecessary to compute embeddings for redundant simplices in traditional tasks.

## 3 Preliminaries

The background knowledge required to present this work better is illustrated in this section. Let  $\mathcal{G} = (\mathcal{V}, \mathcal{E})$  denote an undirected pairwise graph with a finite node set  $\mathcal{V} = \{v_1, \dots, v_n\}$  and an edge set  $\mathcal{E} \subseteq \mathcal{V} \times \mathcal{V}$ . Assume that  $|\mathcal{V}| = n$ ,  $|\mathcal{E}| = n_1$ , and  $N(v)$  denotes the set of nodes adjacent to node  $v$  in  $\mathcal{G}$ , i.e.,  $N(v) = \{u \in \mathcal{V} | (v, u) \in \mathcal{E}\}$ . The nodes are associated with a node feature matrix  $X \in \mathbb{R}^{n \times d}$ , where  $d$  signifies the number of features per node.

Simplicial complexes (Battiston et al. 2020) are a potent tool with a rich theory foundation upon algebraic and differential topology and geometry. Instead of predominantly studying pairwise interactions, the simplicial description facilitates the modeling of higher-order interactions and multi-node graph structures.

**Definition 3.1** (Simplicial complexes, SCs). A simplicial complex  $\mathcal{K}$  is a finite collection of node subsets closed under the operation of taking nonempty subsets, and such a node subset  $\sigma \in \mathcal{K}$  is called a simplex (as illustrated in Figure 1).

A node subset  $\sigma = [v_0, v_1, \dots, v_p] \in \mathcal{K}$  with cardinality  $p + 1$  is referred to as a  $p$ -dimensional simplex, termed  $p$ -simplex, and we denote the set of all such  $p$ -simplices as  $\mathcal{K}_p$  with  $|\mathcal{K}_p| = n_p$ . If the triangle  $[v_1, v_2, v_3] \in \mathcal{K}$ , then we require that all its nonempty subsets  $[v_1]$ ,  $[v_2]$ ,  $[v_3]$ ,  $[v_1, v_2]$ ,  $[v_1, v_3]$ ,  $[v_2, v_3]$  belong to  $\mathcal{K}$ . One can regard vertices as 0-simplices, edges as 1-simplices, “filled” triangles as 2-simplices, and so forth. Pairwise graphs can be viewed as 1-dimensional SCs. In contrast, higher-order SCs generally carry more structure information over pairwise graphs, which is critical and should not be omitted. The boundary relation describes which simplices lie on the boundary of other simplices. For example, vertices  $[v_1]$ ,  $[v_2]$  are on the boundary of edge  $[v_1, v_2]$ , while edge  $[v_1, v_2]$  lies on the boundary of triangle  $[v_1, v_2, v_3]$ .

**Definition 3.2** (Boundary incidence relation). For two simplices  $\sigma$  and  $\tau$ , we say  $\sigma \prec \tau$  iff  $\sigma \subset \tau$  and  $\dim(\sigma) = \dim(\tau) - 1$ .

Model	Convolution Filter	Spectral Domain	Hyperparams	Learnable
GCN (Kipf and Welling 2017)	$(1 - \lambda)^K$	Graph Laplacian	$K$	-
APPP (Gasteiger, Bojchevski, and Günnemann 2019)	$\sum_{k=0}^K \frac{\gamma^k}{1-\gamma} (1-\lambda)^k$	Graph Laplacian	$\gamma, K$	-
GPRGNN (Chien et al. 2020)	$\sum_{k=0}^K \gamma_k (1-\lambda)^k$	Graph Laplacian	$K$	$\gamma_k$
ChebNet (Defferrard, Bresson, and Vandergheynst 2016)	$\sum_{k=0}^K \gamma_k \cos(k \arccos(1-\lambda))$	Graph Laplacian	$K$	$\gamma_k, K$
SNN (Ebli, Defferrard, and Spreemann 2020)	$\lambda^K$	Hodge Laplacian	$K$	-
SCoNe (Roddenberry, Glaze, and Segarra 2021)	$\lambda_{down}^K, \lambda_{up}^K$	Hodge Laplacian	$K$	-
SCNN (Yang, Isufi, and Leus 2022)	$\sum_{k=0}^{K_1} \gamma_{d,k} \lambda_{down}^k + \sum_{k=0}^{K_2} \gamma_{u,k} \lambda_{up}^k$	Hodge Laplacian	$\gamma_{d,k}, \gamma_{u,k}, K_1, K_2$	-
BScNets (Chen, Gel, and Poor 2022)	$f(\lambda_1, \lambda_2, \dots, \lambda_P; \theta)^K$	Block Hodge Laplacian	$K, P$	$\theta$
<b>HiGCN (Ours)</b>	$\sum_{k=0}^K \gamma_{p,k} (1-\lambda_p)^k, p = 1, 2, \dots, P$	FP Laplacian	$K, P$	$\gamma_{p,k}$

Table 1: The filter forms of spectral graph convolutional networks.

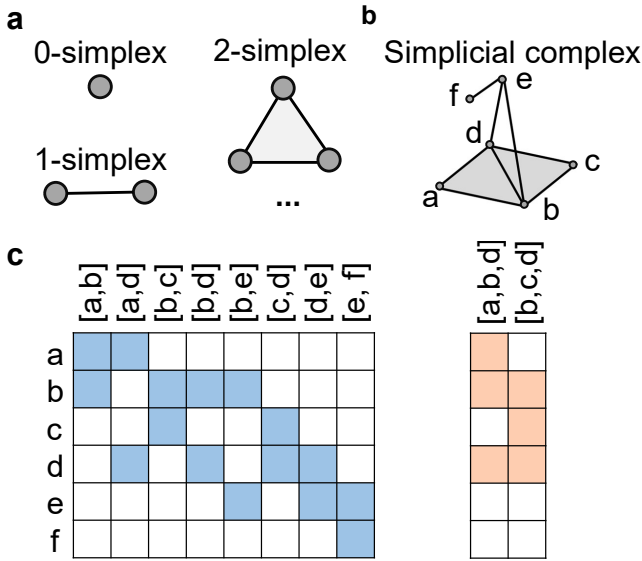


Figure 1: **a** shows several typical simplices, and the collection of simplices forms SCs in **b**. Subfigure **c** visualizes the higher-order incidence matrices  $\mathcal{H}_p$ , where  $p = 1$  for the left panel and  $p = 2$  for the right.

**Hasse diagram.** It is one of the most common representations of SCs, where each vertex corresponds to a simplex. The edges in the Hasse diagram are defined by the boundary incidence relation, and there exists an edge connecting two vertices  $\sigma_1$  and  $\sigma_2$ , iff  $\sigma_1 \prec \sigma_2$ . The hasse diagram is highly expressive, and several simplicial GNNs (Roddenberry, Glaze, and Segarra 2021; Bodnar et al. 2021; Hajij et al. 2022) are built precisely on the boundary incidence relationships shown in the hasse diagram.

**Clique complex lifting.** We can obtain a clique complex, a kind of SCs, by extracting all cliques from a graph and regarding them as simplices. This implies that an empty triangle (owning  $[v_1, v_2]$ ,  $[v_1, v_3]$ ,  $[v_2, v_3]$  but without  $[v_1, v_2, v_3]$ ) cannot occur in clique complexes. The transition from a pairwise graph to a clique complex, termed the clique complex lifting transition, enables us to study pairwise graphs from

simplicial perspectives.

## 4 Higher-order graph convolutional network

We first introduce the higher-order flower-petals model for simplicial complex representation, which will subsequently be leveraged to construct our HiGCN model.

### 4.1 Flower-petals model

Hasse diagrams are valuable in studying SCs, but they are inherently constrained to modeling interactions for directly adjacent simplices and are computationally expensive to construct. Multiple transitions are required for information to pass between nodes and higher-order structures. Besides, the number of total simplices grows exponentially with the number of nodes in dense graphs (Bomze et al. 1999). Computing embeddings for all higher-order structures can be costly and unnecessary for specific-level tasks. To address these challenges, we construct a novel higher-order representation, named the flower-petals (FP) model, and then introduce higher-order FP adjacency and Laplacian matrices based on the higher-order random walk dynamics between the flower core and petals.

It can be simplified only to consider the interaction between 0-simplices and higher-order structures when tackling the most common tasks: node-level tasks. Hence, we construct a flower-petals model by simplifying the intermediate vertices on the Hasse diagram. Specifically, the flower-petals model consists of one core and several petals, see Figure 2(a), with interactions considered only between the core and petals. 0-simplices are placed in the flower core, and each flower petal involves simplices of the same order (larger than zero). The term  $p$ -petal is used to represent the petal containing  $p$ -simplices. Diverse and complex interactions exist between  $p$ -petal and the core, which can be unwrapped as a bipartite graph  $\mathcal{G}_p$ , as shown in Figure 2(b). Mathematically, the bipartite graph  $\mathcal{G}_p$  consists of two distinct vertex sets  $(\mathcal{V}, \mathcal{K}_p)$ , where  $\mathcal{V}$  represents the set of nodes contained in the flower core and  $\mathcal{K}_p$  comprised of simplices in the  $p$ -petal ( $p \geq 1$ ). If simplex  $\sigma (\in \mathcal{K}_p)$  contains node  $v (\in \mathcal{V})$ , then there exists an edge between their corresponding vertices in  $\mathcal{G}_p$ .

The proposed flower-petals model prunes the information interaction rules between petals but is still extremely expres-

sive and useful. Since it is costly to enumerate all simplices (Bomze et al. 1999), we can further accelerate computation by incorporating finite petals in the FP model, that is, by constraining the order of the simplices under consideration.

Inspired by incidence matrices in pairwise networks (Nuffelen 1976), we introduce higher-order incidence matrix  $\mathcal{H}_p \in \mathbb{R}^{|\mathcal{V}| \times |\mathcal{K}_p|}$ . The incidence matrix describes the association between vertices in the core and higher-order structures in the  $p$ -petal, with entry  $\mathcal{H}_p(v, \sigma) = 1$  indicating the vertex  $v$  is contained in the simplex  $\sigma \in \mathcal{K}_p$ . See Figure 1(c) for visual representations.

## 4.2 Flower-petals algebraic description

Hodge Laplacian (Schaub et al. 2020; Hatcher 2002) is a fundamental tool in simplicial complexes. However, it can only describe interactions between simplices within one-order differences. To model interactions between different order simplices more flexibly, we introduce novel matricial descriptions for simplicial complexes based on the random walk dynamics between the flower core and petals.

The main idea of random walks is to traverse a graph starting from a single node or a set of nodes and get sequences of locations. We introduce the traditional random walk model in Appendix D. Walking on the bipartite graphs  $\mathcal{G}_p$  consists of two sub-steps: (I) upward walk and (II) downward walk. The upward walk refers to the walk from nodes in the flower core to their corresponding simplices in the  $p$ -petal, while the downward walk proceeds in the opposite direction.

Suppose  $\pi_\sigma(t)$  encodes the probability for simplex  $\sigma$  to be occupied by a random walker at step  $t$ . In the upward walk process, information is transmitted from vertex to simplex and the probability of moving from vertex  $u$  to simplex  $\sigma$  is equal to  $\mathcal{H}_p(u, \sigma)/d_p(u)$ . The downward walk, i.e., petals-to-core walk, allows information to be transferred from simplices back to nodes. These two processes follow that

$$\pi_\sigma(t-1) = \sum_u \frac{\mathcal{H}_p(u, \sigma)}{d_p(u)} \pi_u(t-2), \quad (1)$$

$$\pi_v(t) = \sum_\sigma \frac{\mathcal{H}_p(v, \sigma)}{\delta_p(\sigma)} \pi_\sigma(t-1). \quad (2)$$

Here,  $d_p(u) = \sum_{\sigma \in \mathcal{K}_p} \mathcal{H}_p(u, \sigma)$  denotes the degree of vertex  $u$  on  $\mathcal{G}_p$ , and  $\delta_p(\sigma)$  represents the degree of  $p$ -simplex  $\sigma$  on  $\mathcal{G}_p$  ( $p \geq 1$ ). Mathematically  $\delta_p(\sigma) = \sum_{v \in \mathcal{V}} \mathcal{H}_p(v, \sigma) = p + 1$ .

The two-step walk integrates both the upward and downward walks, allowing the information to be transmitted from the flower core and back through the petals. A complete two-step walk process necessitates that the last step be a positive even number, and this entire process follows that

$$\pi_v(t) = \sum_\sigma \frac{\mathcal{H}_p(v, \sigma)}{\delta_p(\sigma)} \sum_u \frac{\mathcal{H}_p(u, \sigma)}{d_p(u)} \pi_u(t-2). \quad (3)$$

Let  $\pi(t) = (\pi_{v_1}(t), \dots, \pi_{v_n}(t))^\top$ , we can further derive the matrix representation for the two-step walk as  $\pi(t) = \mathcal{H}_p D_{p,h}^{-1} \mathcal{H}_p^\top D_{p,v}^{-1} \pi(t-2)$ , where  $D_{p,v} = \text{diag}(d_p(v_1), \dots, d_p(v_n))$  and  $D_{p,h} =$

$\text{diag}(\delta_p(\sigma_1), \dots, \delta_p(\sigma_{|\mathcal{K}_p|}))$ . Subsequently, by multiplying  $D_{p,v}^{-1/2}$  from the left sides of this equation, we can obtain

$$D_{p,v}^{-1/2} \pi(t) = \left[ D_{p,v}^{-1/2} \mathcal{H}_p D_{p,h}^{-1} \mathcal{H}_p^\top D_{p,v}^{-1/2} \right] D_{p,v}^{-1/2} \pi(t-2). \quad (4)$$

Therefore, based on the two-step walk dynamic between the flower core and petals, we can define higher-order flower-petals (FP) adjacency matrices analogously to the reduced adjacency matrices (see Appendix D) as

$$\begin{aligned} \tilde{\mathcal{A}}_p &= D_{p,v}^{-1/2} \mathcal{H}_p D_{p,h}^{-1} \mathcal{H}_p^\top D_{p,v}^{-1/2} \\ &= \frac{1}{p+1} D_{p,v}^{-1/2} \mathcal{H}_p \mathcal{H}_p^\top D_{p,v}^{-1/2}. \end{aligned} \quad (5)$$

The latter equality holds since the higher-order structures in each petal belong to the same order, and thus  $D_{p,h} = \text{diag}(p+1, p+1, \dots, p+1) = (p+1)I$ .

The Laplacian operator is crucial for the processing of relational data, and it bears resemblance to the Laplace-Beltrami operator in differential geometry. On the basis of the FP adjacency matrices, we can likewise define a series of higher-order FP Laplacian operators as  $\mathcal{L}_p = I - \tilde{\mathcal{A}}_p$ .

**Theorem 4.1.** *The flower-petals adjacency matrices  $\tilde{\mathcal{A}}_p$  and flower-petals Laplacian matrices  $\mathcal{L}_p$  are all symmetric positive semidefinite.*

It follows from Theorem 4.1 that  $0 \leq \lambda(\tilde{\mathcal{A}}_p), \lambda(\mathcal{L}_p) \leq 1$ . We defer the proof and further theoretical analysis of the spectral properties to Appendix A. Theorem 4.1 contributes in alleviating the numerical instability and exploding/vanishing gradients that may arise in the implementation of deep GNNs based on the FP Laplacians. The diverse FP Laplacian matrices capture the various connectivity relations of the simplicial complexes, where we can learn a series of diverse spectral convolution operators.

## 4.3 Higher-order spectral convolutions

The eigen decomposition  $\mathcal{L} = \Phi \Lambda \Phi^\top$  can be employed on the Laplacian matrix to obtain the orthonormal eigenvectors  $\Phi = (\phi_1, \phi_2, \dots, \phi_n)$  and a diagonal matrix  $\Lambda = \text{diag}(\lambda_1, \lambda_2, \dots, \lambda_n)$ . Then, for a graph signal  $x$ , the graph Fourier transform is defined as  $\Phi^\top x$  (Shuman et al. 2013), where the eigenvectors can be regarded as the Fourier bases and the eigenvalues are interpreted as frequencies. The spectral convolution of signal  $x$  and filter  $g$  can then be formulated as

$$g \star x = \Phi \left( (\Phi^\top g) \odot (\Phi^\top x) \right) = \Phi g(\Lambda) \Phi^\top x. \quad (6)$$

Here, operator  $\odot$  presents the Hadamard product and the filter  $g(\Lambda)$  applies  $g$  element-wisely to the diagonal entries of  $\Lambda$ , i.e.,  $g(\Lambda) = \text{diag}(g(\lambda_1), \dots, g(\lambda_n))$ . Note that spectral decomposition for large-scale networks is computationally expensive, and one can approximate any graph filter using a polynomial filter with enough terms (Shuman et al. 2013; He et al. 2021). Hence, the filter  $g$  is usually set to be a truncated polynomial  $g(\lambda) := \sum_{k=0}^K \gamma_k \lambda^k$  of order  $K$ . In this way, spectral decomposition is avoided, and the convolution

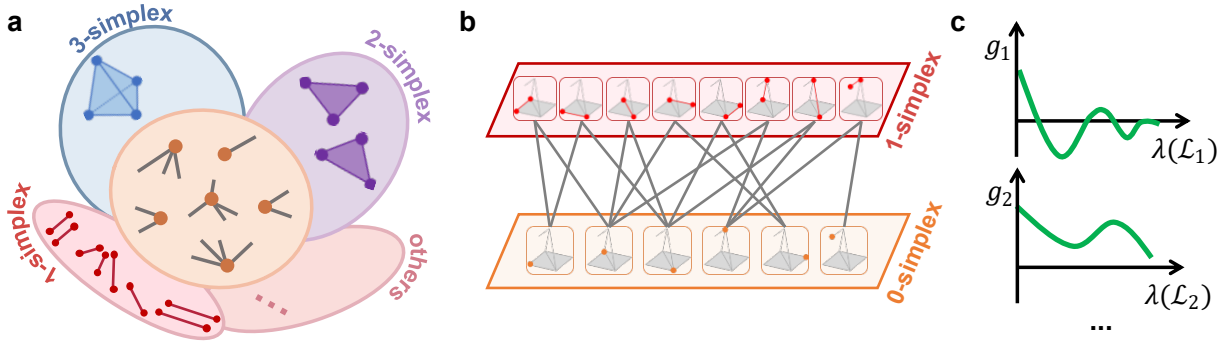


Figure 2: **An illustration of the flower-petals model for SCs.** **a** displays the flower-petals model. The interactions between petals and the core can be unwrapped as a bipartite graph, as depicted in **b**. **c** visualizes the learnable convolutional filters  $g_p$  derived from different flower-petals (FP) Laplacians, which are constructed based on two-step random walk dynamics on **b**.

process can be expressed as  $g \star x = \sum_{k=0}^K \gamma_k \Phi \Lambda^k \Phi^\top x = \sum_{k=0}^K \gamma_k \mathcal{L}^k x$ .

We can obtain different FP Laplacian matrices based on the FP model, which reflect the different connectivity relations of SCs. By defining  $g_p(\mathcal{L}_p) = \sum_{k=0}^K \gamma_{p,k} \mathcal{L}_p^k$ , we can define different convolution operations on each FP Laplacian basis as

$$g \star_p x = g_p(\mathcal{L}_p)x, \quad (7)$$

where  $\star_p$  denotes convolution on the FP Laplacian  $\mathcal{L}_p$ . We summarize some common filter forms of spectral GNNs in Table 1. When processing a simplicial signal  $X \in \mathbb{R}^{n \times d}$  with  $d$  dimensional features, a more general form of spectral GNNs follows that  $Y = \rho(g(\mathcal{L})\varphi(X))$ . Here,  $g$  stands for graph filter, and  $\rho, \varphi$  are permutation-invariant functions.

To encode multi-scale higher-order information, we can obtain the final prediction by concatenating results from different convolution operations as

$$Y_p = g_p(\mathcal{L}_p)\varphi_p(X), \quad Y = \rho\left(\left\|_{p=1}^P Y_p\right.\right). \quad (8)$$

Here,  $\|$  concatenates the representation in different spectral domains. We let the graph filter  $g_p(\mathcal{L}_p) = \sum_{k=0}^K \gamma_{p,k} \mathcal{L}_p^k$  to be different learnable polynomial functions in each FP spectral domain. The learnable polynomial coefficients  $\gamma_{p,k}$  depend on the contributions of different steps in each order.  $K$  is a hyperparameter denoting the largest steps of the simplices that are considered. Besides, we simplify  $\rho$  and  $\varphi$  to linear functions as suggested in (Wang and Zhang 2022), and thus we can obtain

$$Y = \left\|_{p=1}^P \left( \sum_{k=0}^K \gamma_{p,k} \tilde{A}_p^k X \Theta_p \right) W. \quad (9)$$

Here,  $\gamma_{p,k}, \Theta_p$ , and  $W$  are trainable parameters, and  $P$  is a hyperparameter that denotes the highest order of the simplices under consideration. Note that the training process can be accelerated by precalculating  $\tilde{A}_p^k$ , which can be efficiently calculated between sparse matrices.

HiGCN facilitates the independent and flexible learning of filter shapes across disparate FP spectral domains rather than predetermining filter configurations. Consequently, it

is adept at handling both high- and low-frequency signal components in a versatile manner. Furthermore, we find that the filters' weights in different orders quantify the strength of the higher-order interactions, contributing to the understanding of higher-order mechanisms inherent within complex systems.

**Expressive power.** We have developed the HiGCN model from a spectral perspective. The Weisfeiler-Lehman (WL) test (Weisfeiler and Leman 1968) provides a well-studied framework for unique node labeling, and an intrinsic theoretical connection has been uncovered between the WL test and message-passing-based GNNs (Xu et al. 2019; Morris et al. 2019). We extend this relation and propose a higher-order WL test, termed HWL, along with its simplified version SHWL. Detailed procedures for WL, HWL, and SHWL are elaborated in Appendix B. Furthermore, we revisit the HiGCN model from the message-passing perspective in Appendix B, offering an alternative interpretation that underscores the exceptional expressive power of our model.

**Theorem 4.2.** *SHWL with clique complex lifting is strictly more powerful than Weisfeiler-Lehman (WL) test.*

The proposed model can be interpreted as a neural version of the SHWL test where colors are replaced by continuous feature vectors. Moreover, Theorem 4.2 implies that HiGCN endows with greater potential than vanilla GNNs. See Appendix B for proof and detailed discussion.

**Relation to GCN models.** HiGCN shows superiority over pairwise graph-based GCN models for exploiting higher-order information, and it generalizes spectral convolution operations on pairwise graphs, including GCN (Kipf and Welling 2017) and GPRGNN (Chien et al. 2020). On the other hand, HiGCN exhibits greater flexibility than certain Hodge Laplacian-based simplicial GCN models, such as SNN (Ebli, Defferrard, and Spreemann 2020) and SCNN (Yang, Isufi, and Leus 2022), overcoming the constraints of information exchange exclusively through boundary operators. Further derivation and in-depth discussion are presented in Appendix C.

**Symmetries.** Given a pairwise graph  $\mathcal{G}$  characterized by adjacency matrix  $A$  and feature matrix  $X$ , a func-

tion  $f$  is (node) permutation equivariant if  $\mathbf{P}f(A, X) = f(\mathbf{P}A\mathbf{P}^\top, \mathbf{P}X)$  for any permutation operation  $\mathbf{P}$ . GNNs adhere to this equivariance property, ensuring consistent computation of functions irrespective of node permutations. Generalizing pairwise GNNs, HiGCN demonstrates equivariance with respect to relabeling of simplices, which allows it to exploit symmetries in SCs. To formalize this property, we introduce the concept of simplex permutation equivariance and demonstrate that HiGCN fulfills this definition. See Appendix E for proof and detailed discussions.

**Computational complexity.** A balance between performance and complexity can be achieved by limiting the number of petals  $P$ . We find that a small  $P$  is typically adequate, and considering more petals may result in diminishing marginal utility. Generally, the computational complexity of HiGCN is comparable to that of spectral GNNs. We report the average training time per epoch and average total running time in Table 8, demonstrating that HiGCN achieves competitive performance with a reasonable computational cost. Additionally, when the targeted graph is not in the form of SCs, one should also consider the one-time preprocessing procedure for graph lifting, see Appendix G for details.

## 5 Experiments

In this section, we conduct experiments including node/graph classification and simplicial data imputation on typical datasets to evaluate the performance of HiGCN. Detailed data introduction and experimental settings are deferred to Appendix H and Appendix I, respectively.

### 5.1 Node classification on empirical datasets

We perform the node classification task employing five homogeneous graphs, encompassing three citation graphs — Cora (McCallum et al. 2000), CiteSeer and PubMed (Yang, Cohen, and Salakhudinov 2016) — and two Amazon co-purchase graphs, Computers and Photo (Shchur et al. 2018). Additionally, we include five heterogeneous graphs, namely Wikipedia graphs Chameleon and Squirrel (Rozemberczki, Allen, and Sarkar 2021), the Actor co-occurrence graph, and the webpage graphs Texas and Wisconsin from WebKB (Pei et al. 2020). Adjacent nodes in a homogeneous graph tend to share the same label, while the opposite holds in heterogeneous graphs (Zhu et al. 2020). Besides, the clique complex lifting transition is carried out on each graph, and the statistics of these graphs are summarized in Table 9. HiGCN is compared with various baseline models including MLP, pairwise GNNs (GAT (Veličković et al. 2018), ChebNet (Defferrard, Bresson, and Vandergheynst 2016), BernNet (He et al. 2021), GGCN (Yan et al. 2021), APPNP (Gasteiger, Bojchevski, and Günnemann 2019), and GPRGNN (Chien et al. 2020)), as well as higher-order models (k-simplex2vec (k-S2V) (Hacker 2020), Simplex2vec (S2V) (Billings et al. 2019), SNN (Ebli, Defferrard, and Spreemann 2020), SGAT, and SGATEF (Lee, Ji, and Tay 2022)). We randomly partition the node set into training, validation, and testing subsets at a ratio of 60%, 20%, and 20% respectively, and repeat the experiments 100 times for

each dataset. The mean classification accuracy (the micro-F1 score) along with a 95% confidence interval on the test nodes are reported in Table 2.  $p$ -HiGCN signifies the model under the hyperparameter  $P = p$ .

It can be drawn from Table 2 that HiGCN achieves the best results in 9 out of the 10 graphs. On the remaining dataset, HiGCN also displays comparable performance to the SOTA methods. Generally, 2-HiGCN and 3-HiGCN outperform 1-HiGCN, suggesting that higher-order information is valuable for graph learning. Moreover, HiGCN shows a greater lead on homogeneous graphs on average, consistent with the intuition that higher-order effects tend to manifest on homogeneous graphs (Battiston et al. 2020). Additionally, we scale HiGCN to three larger datasets: two homogeneous graphs (Ogbn-arxiv (Hu et al. 2020) and Genius (Lim and Benson 2021)) and one heterogeneous graph (Penn94 (Traud, Mucha, and Porter 2012)). Table 7 in Appendix G show that our HiGCN model outperforms other methods and has robust scalability.

**Quantification of higher-order strength.** The filter weights  $\gamma_{p,k}$  are related to the impact of  $p$ -simplex on  $k$ -hop neighbors; thus, we quantify the  $p$ -order interaction strength in terms of  $S_p = \sum_k |\gamma_{p,k}|$ . Specifically, we visualize the higher-order strength with the order  $p = 1, 2, 3, 4$  on two homogeneous graphs and two heterogeneous graphs in Figure 3(a)-(d). We observe that  $S_p$  decreases gently with the increase of  $p$  in homogeneous graphs, while it decreases rapidly in heterogeneous graphs. This implies that the strength of higher-order effects varies at different orders and across different types of graphs.

Additionally, we discover that networks with fewer higher-order structures tend to exhibit a smaller  $S_p$ , which may degrade the performance of HiGCN. For instance, in Texas, the only dataset where HiGCN performance is not optimal, we notice that its higher-order interactions are considerably weaker compared to the lower-order interactions (see Figure 3(d)), and it has the fewest triangles among all datasets (see Table 9). To verify this conjecture, we modify the number of higher-order structures by adjusting the connectivity of edges while maintaining the degree distribution in the network as done in 1k null models (Orsini et al. 2015), see Appendix F.1 for details. We define the relative higher-order density for the modified networks as  $\rho_p = n'_p/n_p - 1$ , where  $n_p$  and  $n'_p$  denote the number of  $p$ -simplex in the original and the modified network, respectively. Figure 3(e) and Figure 6 in Appendix F.2 visualize  $S_p$  under different  $\rho_2$  for Texas and Actor, and an upward trend is observed as the triangle density  $\rho_2$  increases. Tables 5 and 6 also show an increasing accuracy rank of HiGCN with the rise of  $\rho_2$ . Additionally, we exclude the effect of parameter initialization on the above conclusions in Appendix F.3. Hence,  $S_p$  can serve as a quantification of  $p$ -order interaction strength. More experimental results and discussions are deferred to Appendix F.

### 5.2 Simplicial data imputation

We employ HiGCN to impute missing signals in coauthorship complexes, a typical simplicial complex, wherein a pa-



Method	Cora	Citeseer	PubMed	Computers	Photo	Chameleon	Actor	Squirrel	Texas	Wisconsin
MLP	76.96±0.95	76.58±0.88	85.94±0.22	82.85±0.38	84.72±0.34	46.85±1.51	40.19±0.56	31.03±1.18	91.45±1.14	93.56±0.87
GAT	88.03±0.79	80.52±0.71	87.04±0.24	83.33±0.38	90.94±0.68	63.90±0.46	35.98±0.23	42.72±0.33	78.87±0.86	65.64±1.74
ChebNet	86.67±0.82	79.11±0.75	87.95±0.28	87.54±0.43	93.77±0.32	59.96±0.51	38.02±0.23	40.67±0.31	86.08±0.96	90.57±0.91
BernNet	88.52±0.95	80.09±0.79	88.48±0.41	87.64±0.44	93.63±0.35	<u>68.29</u> ±1.58	<u>41.79</u> ±1.91	<u>51.35</u> ±0.73	<b>93.12</b> ±0.65	91.82±0.38
GGCN	87.68±1.26	77.08±1.32	89.63±0.46	N/A	89.92±0.97	62.72±2.05	38.09±0.88	49.86±1.55	85.81±1.72	87.65±1.50
APPNP	88.14±0.73	80.47±0.74	88.12±0.31	85.32±0.37	88.51±0.31	51.89±1.82	39.66±0.55	34.71±0.57	90.98±1.64	64.59±0.97
GPRGNN	88.57±0.69	80.12±0.83	88.46±0.33	86.85±0.25	93.85±0.28	67.28±1.09	39.92±0.67	50.15±1.92	<u>92.95</u> ±1.31	88.54±1.37
k-S2V	68.30±0.35	44.22±0.44	67.21±0.41	84.15±0.11	89.08±0.65	49.00±0.82	N/A	39.15±0.49	85.12±0.98	87.44±0.77
S2V	80.15±0.88	78.21±0.34	85.48±0.33	83.25±0.50	84.33±0.19	47.14±0.32	39.22±0.50	40.26±0.74	82.12±0.23	83.48±0.89
SNN	87.13±1.02	79.87±0.68	86.73±0.28	83.33±0.32	88.27±0.74	60.96±0.78	30.59±0.23	45.66±0.39	75.16±0.96	61.93±0.83
SGAT	77.49±0.79	78.93±0.63	88.10±0.59	N/A	N/A	51.23±0.36	36.71±0.49	N/A	89.83±0.66	81.47±0.64
SGATEF	78.12±0.85	79.16±0.72	88.47±0.62	N/A	N/A	51.61±0.40	37.33±0.58	N/A	89.67±0.74	81.59±0.81
1-HiGCN	88.96±0.28	<u>80.96</u> ±0.27	89.83±0.73	90.50±0.52	<u>95.22</u> ±0.30	63.55±0.84	41.57±0.27	49.13±0.33	90.36±0.78	94.39±0.94
2-HiGCN	89.33±0.23	<b>81.12</b> ±0.28	<u>89.89</u> ±0.16	<b>90.76</b> ±0.27	<b>95.33</b> ±0.37	<b>68.47</b> ±0.45	<b>41.81</b> ±0.52	<b>51.86</b> ±0.42	92.45±0.73	<u>94.69</u> ±0.95
3-HiGCN	89.00±0.26	80.90±0.22	89.73±0.17	90.65±0.20	94.40±0.31	67.12±0.32	41.29±0.20	50.92±0.34	91.85±0.62	94.12±0.68
4-HiGCN	88.63±0.28	80.47±0.31	<b>89.95</b> ±0.13	90.35±0.31	94.10±0.24	66.98±0.23	41.13±0.24	50.45±0.21	91.42±0.75	<b>94.99</b> ±0.65

Table 2: Node classification results on empirical benchmark networks: mean accuracy (%)  $\pm$  95% confidence interval. The best results are in bold, while the second-best ones are underlined.

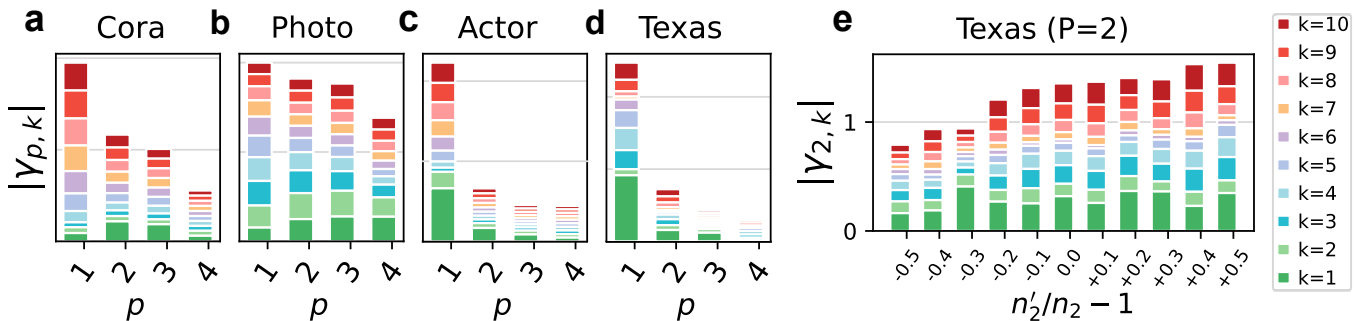


Figure 3: **a**, **b**, **c** and **d** visualizes the stack of learned weights  $|\gamma_{p,k}|$  under order  $p = 1, 2, 3, 4 (P = 4)$ . **e** visualizes the stack of  $|\gamma_{2,k}|$  for Texas under various relative triangle densities  $\rho_2$ .

per with  $p + 1$  authors is represented by a  $p$ -simplex, and the  $p$ -simplicial signal corresponds to the number of collaborative publications among authors in the  $p$ -simplex. We extract three coauthorship complexes from DBLP (Benson et al. 2018), History and Geology (Sinha et al. 2015), respectively (refer to Appendix H). In this experiment, the known signals for 0-simplex are set to range from 10% to 70% (in units of 20%), and the remainders are regarded as missing signals, replaced by the median of known signals. We apply Kendall’s Tau  $\mathcal{T}$  to measure the correlation between true and predicted simplicial signal, with  $\mathcal{T}$  approaching 1 indicating superior imputation performance (Kendall 1938). The experiment is repeated for 10 different random weight initializations, and the results are compared against higher-order models (namely SNN (Ebli, Defferrard, and Spremann 2020), SGAT, and SGATEF (Lee, Ji, and Tay 2022)), as summarized in Table 3. Our results demonstrate that HiGCN outperforms these higher-order benchmarks. This is mainly due to the inherent flexibility of our FP model in capturing higher-order information, while the benchmarks are restricted to learning through upper or lower adjacencies. Besides, SGAT and SGATEF are optimally designed

for heterogeneous networks, a category unsuitable for coauthorship complexes, thereby leading to inferior performance. Moreover, HiGCN achieves significant performance gains especially when less information is known. This may be attributed to higher-order information compensating for missing signals, while an overlap may occur when the known information is abundant.

### 5.3 Graph classification on TUD benchmarks

To verify the broad applicability of the proposed model, we also evaluate the graph classification performance of HiGCN using various datasets from diverse domains, which are categorized into two main groups: bioinformatics datasets (i.e., PROTEINS (Borgwardt et al. 2005), MUTAG (Debnath et al. 1991), PTC (Toivonen et al. 2003)) and social network datasets (i.e., IMDB-B, IMDB-M (Yanardag and Vishwanathan 2015)). To obtain a global embedding for graph classification, we apply readout operations by performing averaging or summation. Following the standard pipeline in (Xu et al. 2019), we conduct a 10-fold cross-validation procedure and report the maximum average validation accuracy across folds. The performance of

SCs Method	10%	30%	50%	70%	
History	SNN	0.201±0.013	0.354±0.016	0.495±0.002	0.661±0.002
	SGAT	0.180±0.010	0.330±0.002	0.432±0.016	0.602±0.005
	SGATEF	0.200±0.002	0.340±0.017	0.454±0.021	0.633±0.012
	<b>HiGCN</b>	<b>0.258±0.004</b>	<b>0.438±0.002</b>	<b>0.579±0.005</b>	<b>0.666±0.009</b>
Geology	SNN	0.265±0.022	0.417±0.004	0.594±0.02	0.704±0.003
	SGAT	0.223±0.004	0.345±0.030	0.599±0.009	0.631±0.008
	SGATEF	0.230±0.002	0.369±0.018	0.615±0.031	0.682±0.012
	<b>HiGCN</b>	<b>0.463±0.012</b>	<b>0.565±0.007</b>	<b>0.644±0.014</b>	<b>0.708±0.002</b>
DBLP	SNN	0.222±0.021	0.348±0.008	0.496±0.005	0.668±0.003
	SGAT	0.210±0.015	0.279±0.054	0.487±0.022	0.643±0.017
	SGATEF	0.223±0.004	0.311±0.002	0.491±0.008	0.678±0.005
	<b>HiGCN</b>	<b>0.385±0.011</b>	<b>0.511±0.004</b>	<b>0.587±0.021</b>	<b>0.685±0.002</b>

Table 3: Simplicial data imputation results: mean Kendall correlation  $\pm$  standard deviation. The best results are highlighted in bold.

Dataset	PROTEINS	MUTAG	PTC	IMDB-B	IMDB-M
RWK	59.6±0.1	79.2±2.1	55.9±0.3	N/A	N/A
GK (k=3)	71.4±0.3	81.4±1.7	55.7±0.5	N/A	N/A
PK	73.7±0.7	76.0±2.7	59.5±2.4	N/A	N/A
WL kernel	75.0±3.1	90.4±5.7	59.9±4.3	73.8±3.9	50.9±3.8
DCNN	61.3±1.6	N/A	N/A	49.1±1.4	33.5±1.4
DGCNN	75.5±0.9	85.8±1.8	58.6±2.5	70.0±10.9	47.8±10.9
IGN	76.6±5.5	83.9±13.0	58.5±6.9	72.0±5.5	48.7±3.4
GIN	76.2±2.8	89.4±5.6	64.6±7.0	75.1±5.1	52.3±2.8
PPGNs	<b>77.2±4.7</b>	<b>90.6±8.7</b>	<b>66.2±6.6</b>	73.0±15.8	50.5±3.6
Natural GN	71.7±1.0	89.4±1.6	<b>66.8±1.7</b>	73.5±2.0	51.3±1.5
MPSN	76.7±4.6	89.8±5.5	61.8±9.1	75.6±3.2	52.4±2.9
<b>HiGCN</b>	<b>77.0±4.2</b>	<b>91.5±6.4</b>	<b>66.2±6.9</b>	<b>76.2±5.1</b>	<b>52.7±3.5</b>

Table 4: Graph classification results on the TUDatasets benchmark.

HiGCN is presented in Table 4, alongside the results for kernel methods (RWK (Gärtner, Flach, and Wrobel 2003), GK (Shervashidze et al. 2009), PK (Neumann et al. 2016), WL kernel (Shervashidze et al. 2011)), pairwise GNNs (DCNN (Atwood and Towsley 2016), DGCNN (Zhang et al. 2018), IGN (Maron et al. 2018), GIN (Xu et al. 2019), PPGNs (Maron et al. 2019), Natural GN (de Haan, Cohen, and Welling 2020)), and the higher-order model MPSN (Bodnar et al. 2021). Our model exhibits superior performance compared to the baselines, demonstrating strong empirical results across all benchmark datasets. Additionally, HiGCN achieves its optimal outcomes on the two social network datasets, coinciding with the conclusion that simplices play a pivotal role in social networks (Battiston et al. 2021).

## 6 Conclusion

This paper introduces a novel higher-order representation, the flower-petals (FP) model, enabling interactions among simplices of arbitrary orders. Higher-order FP adjacency and Laplacian matrices are further introduced based on the higher-order random walk dynamics between the flower core and petals. As the application of FP Laplacians in deep learning, a higher-order graph convolutional network

(HiGCN) framework is proposed for graph learning. Our theoretical analysis highlights HiGCN’s enhanced expressive power, which is supported by empirical performance gains across various graph tasks. Moreover, we deploy a data-driven strategy to demonstrate the existence of higher-order interactions and to quantify their interaction strength. To increase efficiency, we simplify the interaction rules in the SCs, allowing information transfer only between the flower core and petals. It is a valuable and interesting question whether other simplifications would be more effective for specific tasks. This work promises to offer novel insights and serve as a potent tool in higher-order network analysis.

## Acknowledgements

The authors acknowledge the STI 2030—Major Projects (Grant No. 2022ZD0211400), the National Natural Science Foundation of China (Grant No. T2293771), the Sichuan Science and Technology Program (Grant No. 2023NS-FSC1919), and the New Cornerstone Science Foundation through the XPLORER PRIZE.

## References

- Atwood, J.; and Towsley, D. 2016. Diffusion-convolutional neural networks. *Advances in neural information processing systems*, 29.
- Battiston, F.; Amico, E.; Barrat, A.; Bianconi, G.; Ferraz de Arruda, G.; Franceschiello, B.; Iacopini, I.; Kéfi, S.; Latora, V.; Moreno, Y.; et al. 2021. The physics of higher-order interactions in complex systems. *Nature Physics*, 17(10): 1093–1098.
- Battiston, F.; Cencetti, G.; Iacopini, I.; Latora, V.; Lucas, M.; Patania, A.; Young, J.-G.; and Petri, G. 2020. Networks beyond pairwise interactions: Structure and dynamics. *Physics Reports*, 874: 1–92.
- Benson, A. R.; Abebe, R.; Schaub, M. T.; Jadbabaie, A.; and Kleinberg, J. 2018. Simplicial closure and higher-order link prediction. *Proceedings of the National Academy of Sciences*.
- Billings, J. C. W.; Hu, M.; Lerda, G.; Medvedev, A. N.; Mottes, F.; Onicas, A.; Santoro, A.; and Petri, G. 2019. Simplex2vec embeddings for community detection in simplicial complexes. *arXiv preprint arXiv:1906.09068*.
- Bodnar, C.; Frasca, F.; Wang, Y.; Otter, N.; Montufar, G. F.; Lio, P.; and Bronstein, M. 2021. Weisfeiler and Lehman go topological: Message passing simplicial networks. In *International Conference on Machine Learning (ICML)*, 1026–1037.
- Bomze, I. M.; Budinich, M.; Pardalos, P. M.; and Pelillo, M. 1999. The maximum clique problem. In *Handbook of combinatorial optimization*, 1–74. Springer.
- Borgwardt, K. M.; Ong, C. S.; Schönauer, S.; Vishwanathan, S.; Smola, A. J.; and Kriegel, H.-P. 2005. Protein function prediction via graph kernels. *Bioinformatics*, 21(suppl\_1): i47–i56.
- Bron, C.; and Kerbosch, J. 1973. Algorithm 457: Finding All Cliques of an Undirected Graph. *Commun. ACM*, 16(9): 575–577.



- Bruna, J.; Zaremba, W.; Szlam, A.; and LeCun, Y. 2014. Spectral networks and deep locally connected networks on graphs. In *2nd International Conference on Learning Representations, ICLR*.
- Cai, J.; Fürer, M.; and Immerman, N. 1992. An optimal lower bound on the number of variables for graph identification. *Combinatorica*, 12(4): 398–140.
- Centola, D. 2010. The Spread of Behavior in an Online Social Network Experiment. *Science*, 329(5996): 1194–1197.
- Chen, Y.; Gel, Y. R.; and Poor, H. V. 2022. BScNets: Block Simplicial Complex Neural Networks. *Proceedings of the AAAI Conference on Artificial Intelligence*, 36(6): 6333–6341.
- Chiba, N.; and Nishizeki, T. 1985. Arboricity and subgraph listing algorithms. *SIAM J. Comput.*, 14(1): 210–223.
- Chien, E.; Peng, J.; Li, P.; and Milenkovic, O. 2020. Adaptive Universal Generalized PageRank Graph Neural Network. In *International Conference on Learning Representations*.
- de Haan, P.; Cohen, T. S.; and Welling, M. 2020. Natural graph networks. *Advances in neural information processing systems*, 33: 3636–3646.
- Debnath, A. K.; Lopez de Compadre, R. L.; Debnath, G.; Shusterman, A. J.; and Hansch, C. 1991. Structure-activity relationship of mutagenic aromatic and heteroaromatic nitro compounds. correlation with molecular orbital energies and hydrophobicity. *Journal of medicinal chemistry*, 34(2): 786–797.
- Defferrard, M.; Bresson, X.; and Vandergheynst, P. 2016. Convolutional neural networks on graphs with fast localized spectral filtering. *Advances in neural information processing systems*, 29: 3838–3845.
- Ebli, S.; Defferrard, M.; and Spreemann, G. 2020. Simplicial Neural Networks. In *NeurIPS 2020 Workshop on Topological Data Analysis and Beyond*.
- Fey, M.; and Lenssen, J. E. 2019. Fast graph representation learning with PyTorch Geometric. *arXiv preprint arXiv:1903.02428*.
- Gambuzza, L. V.; Di Patti, F.; Gallo, L.; Lepri, S.; Romance, M.; Criado, R.; Frasca, M.; Latora, V.; and Boccaletti, S. 2021. Stability of synchronization in simplicial complexes. *Nature communications*, 12(1): 1–13.
- Ganmor, E.; Segev, R.; and Schneidman, E. 2011. Sparse low-order interaction network underlies a highly correlated and learnable neural population code. *Proceedings of the National Academy of Sciences*, 108(23): 9679–9684.
- Gao, Y.; Zhang, Z.; Lin, H.; Zhao, X.; Du, S.; and Zou, C. 2022. Hypergraph Learning: Methods and Practices. *IEEE Transactions on Pattern Analysis and Machine Intelligence*, 44(5): 2548–2566.
- Gärtner, T.; Flach, P.; and Wrobel, S. 2003. On graph kernels: Hardness results and efficient alternatives. In *Learning Theory and Kernel Machines*, 129–143. Springer.
- Gasteiger, J.; Bojchevski, A.; and Günnemann, S. 2019. Predict then Propagate: Graph Neural Networks meet Personalized PageRank. In *International Conference on Learning Representations*.
- Grilli, J.; Barabás, G.; Michalska-Smith, M. J.; and Allesina, S. 2017. Higher-order interactions stabilize dynamics in competitive network models. *Nature*, 548(7666): 210–213.
- Hacker, C. 2020. k-simplex2vec: a simplicial extension of node2vec. *arXiv preprint arXiv:2010.05636*.
- Hajij, M.; Zamzmi, G.; Papamarkou, T.; Maroulas, V.; and Cai, X. 2022. Simplicial complex representation learning. In *Machine Learning on Graphs (MLOG) Workshop at 15th ACM International WSDM Conference*.
- Hatcher, A. 2002. *Algebraic topology*. Cambridge University Press.
- He, M.; Wei, Z.; Xu, H.; et al. 2021. Bernnet: Learning arbitrary graph spectral filters via bernstein approximation. *Advances in Neural Information Processing Systems*, 34: 14239–14251.
- Hu, W.; Fey, M.; Zitnik, M.; Dong, Y.; Ren, H.; Liu, B.; Catasta, M.; and Leskovec, J. 2020. Open graph benchmark: Datasets for machine learning on graphs. *Advances in neural information processing systems*, 33: 22118–22133.
- Kendall, M. G. 1938. A new measure of rank correlation. *Biometrika*, 30(1/2): 81–93.
- Kipf, T. N.; and Welling, M. 2017. Semi-Supervised Classification with Graph Convolutional Networks. In *ICLR*.
- Lee, S. H.; Ji, F.; and Tay, W. P. 2022. SGAT: Simplicial Graph Attention Network. In *Proceedings of the Thirty-First International Joint Conference on Artificial Intelligence (IJCAI-22)*, 3192–3200.
- Lim, D.; and Benson, A. R. 2021. Expertise and dynamics within crowdsourced musical knowledge curation: A case study of the genius platform. In *Proceedings of the International AAAI Conference on Web and Social Media*, volume 15, 373–384.
- Maron, H.; Ben-Hamu, H.; Serviansky, H.; and Lipman, Y. 2019. Provably powerful graph networks. *Advances in neural information processing systems*, 32.
- Maron, H.; Ben-Hamu, H.; Shamir, N.; and Lipman, Y. 2018. Invariant and Equivariant Graph Networks. In *International Conference on Learning Representations*.
- McCallum, A. K.; Nigam, K.; Rennie, J.; and Seymore, K. 2000. Automating the construction of internet portals with machine learning. *Information Retrieval*, 3(2): 127–163.
- Milgram, S. 1967. The small world problem. *Psychology today*, 2(1): 60–67.
- Morris, C.; Ritzert, M.; Fey, M.; Hamilton, W. L.; Lenssen, J. E.; Rattan, G.; and Grohe, M. 2019. Weisfeiler and Leman Go Neural: Higher-Order Graph Neural Networks. *Proceedings of the AAAI Conference on Artificial Intelligence*, 33(01): 4602–4609.
- Neumann, M.; Garnett, R.; Bauckhage, C.; and Kersting, K. 2016. Propagation kernels: efficient graph kernels from propagated information. *Machine Learning*, 102: 209–245.
- Nuffelen, C. V. 1976. On the incidence matrix of a graph. *IEEE Transactions on Circuits and Systems*, 23: 572–572.
- Orsini, C.; Dankulov, M. M.; Colomer-de Simón, P.; Jamakovic, A.; Mahadevan, P.; Vahdat, A.; Bassler, K. E.;

- Toroczkai, Z.; Boguná, M.; Caldarelli, G.; et al. 2015. Quantifying randomness in real networks. *Nature communications*, 6(1): 8627.
- Pei, H.; Wei, B.; Chang, K. C.-C.; Lei, Y.; and Yang, B. 2020. Geom-GCN: Geometric Graph Convolutional Networks. In *International Conference on Learning Representations*.
- Qu, Z.; Huang, Y.; and Zheng, M. 2020. A novel coherence-based quantum steganalysis protocol. *Quantum Information Processing*, 19: 362.
- Roddenberry, T. M.; Glaze, N.; and Segarra, S. 2021. Principled Simplicial Neural Networks for Trajectory Prediction. In *Proceedings of the 38th International Conference on Machine Learning*, volume 139, 9020–9029. PMLR.
- Rozemberczki, B.; Allen, C.; and Sarkar, R. 2021. Multi-scale attributed node embedding. *Journal of Complex Networks*, 9(2): 1–22.
- Schaub, M. T.; Benson, A. R.; Horn, P.; Lippner, G.; and Jadbabaie, A. 2020. Random walks on simplicial complexes and the normalized Hodge 1-Laplacian. *SIAM Review*, 62(2): 353–391.
- Shchur, O.; Mumme, M.; Bojchevski, A.; and Günnemann, S. 2018. Pitfalls of Graph Neural Network Evaluation. *CoRR*, abs/1811.05868.
- Shervashidze, N.; Schweitzer, P.; Van Leeuwen, E. J.; Mehlhorn, K.; and Borgwardt, K. M. 2011. Weisfeiler-lehman graph kernels. *Journal of Machine Learning Research*, 12(9).
- Shervashidze, N.; Vishwanathan, S.; Petri, T.; Mehlhorn, K.; and Borgwardt, K. 2009. Efficient graphlet kernels for large graph comparison. In *Artificial intelligence and statistics*, 488–495. PMLR.
- Shuman, D. I.; Narang, S. K.; Frossard, P.; Ortega, A.; and Vandergheynst, P. 2013. The emerging field of signal processing on graphs: Extending high-dimensional data analysis to networks and other irregular domains. *IEEE Signal Processing Magazine*, 30(3): 83–98.
- Sinha, A.; Shen, Z.; Song, Y.; Ma, H.; Eide, D.; Hsu, B.-J. P.; and Wang, K. 2015. An Overview of Microsoft Academic Service (MAS) and Applications. In *Proceedings of the 24th International Conference on World Wide Web*. ACM Press.
- Sizemore, A. E.; Giusti, C.; Kahn, A.; Vettel, J. M.; Betzel, R. F.; and Bassett, D. S. 2018. Cliques and cavities in the human connectome. *Journal of computational neuroscience*, 44(1): 115–145.
- Toivonen, H.; Srinivasan, A.; King, R. D.; Kramer, S.; and Helma, C. 2003. Statistical evaluation of the predictive toxicology challenge 2000–2001. *Bioinformatics*, 19(10): 1183–1193.
- Traud, A. L.; Mucha, P. J.; and Porter, M. A. 2012. Social structure of facebook networks. *Physica A: Statistical Mechanics and its Applications*, 391(16): 4165–4180.
- Veličković, P.; Cucurull, G.; Casanova, A.; Romero, A.; Liò, P.; and Bengio, Y. 2018. Graph Attention Networks. In *International Conference on Learning Representations (ICLR)*.
- Wang, X.; and Zhang, M. 2022. How Powerful are Spectral Graph Neural Networks. In *International Conference on Machine Learning (ICML)*.
- Weisfeiler, B.; and Leman, A. 1968. The reduction of a graph to canonical form and the algebra which appears therein. *NTI, Series*, 2(9): 12–16.
- Wu, F.; Souza, A.; Zhang, T.; Fifty, C.; Yu, T.; and Weinberger, K. 2019. Simplifying Graph Convolutional Networks. In Chaudhuri, K.; and Salakhutdinov, R., eds., *Proceedings of the 36th International Conference on Machine Learning*, volume 97 of *Proceedings of Machine Learning Research*, 6861–6871. PMLR.
- Wu, S.; Sun, F.; Zhang, W.; Xie, X.; and Cui, B. 2022. Graph Neural Networks in Recommender Systems: A Survey. *ACM Comput. Surv.*
- Xu, K.; Hu, W.; Leskovec, J.; and Jegelka, S. 2019. How powerful are graph neural networks? In *International Conference on Learning Representations (ICLR)*.
- Yan, Y.; Hashemi, M.; Swersky, K.; Yang, Y.; and Koutra, D. 2021. Two sides of the same coin: Heterophily and over-smoothing in graph convolutional neural networks. *arXiv preprint arXiv:2102.06462*.
- Yanardag, P.; and Vishwanathan, S. 2015. Deep Graph Kernels. In *Proceedings of the 21th ACM SIGKDD International Conference on Knowledge Discovery and Data Mining, KDD '15*, 1365–1374. New York, NY, USA: Association for Computing Machinery. ISBN 9781450336642.
- Yang, M.; Isufi, E.; and Leus, G. 2022. Simplicial convolutional neural networks. In *ICASSP*, 8847–8851.
- Yang, R.; Zhou, F.; Liu, B.; and Lü, L. 2023. A generalized simplicial model and its application. *arXiv preprint arXiv:2309.02851*.
- Yang, Z.; Cohen, W.; and Salakhutdinov, R. 2016. Revisiting Semi-Supervised Learning with Graph Embeddings. In *Proceedings of The 33rd International Conference on Machine Learning*, volume 48 of *Proceedings of Machine Learning Research*, 40–48. New York, New York, USA: PMLR.
- Zeng, Y.; Huang, Y.; Ren, X.-L.; and Lü, L. 2023. Identifying vital nodes through augmented random walks on higher-order networks. *arXiv preprint arXiv:2305.06898*.
- Zhang, M.; Cui, Z.; Neumann, M.; and Chen, Y. 2018. An end-to-end deep learning architecture for graph classification. In *Proceedings of the AAAI conference on artificial intelligence*, volume 32.
- Zhu, J.; Yan, Y.; Zhao, L.; Heimann, M.; Akoglu, L.; and Koutra, D. 2020. Beyond homophily in graph neural networks: Current limitations and effective designs. *Advances in Neural Information Processing Systems*, 33: 7793–7804.
- Zitnik, M.; Agrawal, M.; and Leskovec, J. 2018. Modeling polypharmacy side effects with graph convolutional networks. *Bioinformatics*, 34(13): i457–i466.

## Appendix

### A Spectral analysis for flower-petals algebraic descriptions

In this section, we provide a theoretical analysis of the spectral properties of the flower-petals adjacency and Laplacian matrices.

We divide Theorem 4.1 into two separate lemmas and prove them individually.

**Lemma A.1** (Non-negativity of  $\tilde{\mathcal{A}}_p$ ). *The flower-petals adjacency matrices  $\tilde{\mathcal{A}}_p$  are symmetric positive semidefinite.*

*Proof.* By considering the bilinear form  $x^\top \tilde{\mathcal{A}}_p x$ , it can be easily drawn that  $\tilde{\mathcal{A}}_p$  are positive semidefinite:

$$\begin{aligned} x^\top \tilde{\mathcal{A}}_p x &= \frac{1}{p+1} x^\top D_{p,v}^{-1/2} \mathcal{H}_p \mathcal{H}_p^\top D_{p,v}^{-1/2} x \\ &= \frac{1}{p+1} \left( x^\top D_{p,v}^{-1/2} \mathcal{H}_p \right) \left( \mathcal{H}_p^\top D_{p,v}^{-1/2} x \right) \\ &\geq 0. \end{aligned} \quad (10)$$

□

**Lemma A.2** (Non-negativity of  $\mathcal{L}_p$ ). *The flower-petals Laplacian matrices  $\mathcal{L}_p$  are symmetric positive semidefinite.*

*Proof.* We first introduce a matrix  $G_{\sigma_p}$  to support the proof,

$$G_{\sigma_p}(i, j) = \begin{cases} p, & v_i \in \sigma_p, v_j \in \sigma_p, i = j \\ -1, & v_i \in \sigma_p, v_j \in \sigma_p, i \neq j \\ 0, & \text{otherwise} \end{cases}. \quad (11)$$

Let  $\sigma_p = [v_{i_1}, v_{i_2}, \dots, v_{i_{(p+1)}}]$  be an arbitrary  $p$ -simplex, and the notation  $x = (x_1, x_2, \dots, x_n)^\top$  denotes an arbitrary vector in  $\mathbb{R}^n$ . By considering the bilinear form  $x^\top G_{\sigma_p} x$ , we see that  $G_{\sigma_p}$  is positive semidefinite:

$$\begin{aligned} x^\top G_{\sigma_p} x &= x_{i_1} (px_{i_1} - x_{i_2} - \dots - x_{i_{p+1}}) + \\ &\quad x_{i_2} (px_{i_2} - x_{i_1} - \dots - x_{i_{p+1}}) + \dots \\ &= (p+1) \sum_{t=1}^{p+1} x_{i_t}^2 - \left( \sum_{t=1}^{p+1} x_{i_t} \right)^2 \\ &\geq 0. \end{aligned} \quad (12)$$

The last inequality holds exploiting the Cauchy-Schwarz inequality.

We write the higher-order FP Laplacian as a sum over the  $p$ -simplices that

$$\begin{aligned} \mathcal{L}_p &= I - \tilde{\mathcal{A}}_p \\ &= \frac{1}{p+1} D_{p,v}^{-1/2} [(p+1)D_{p,v} - \mathcal{H}_p \mathcal{H}_p^\top] D_{p,v}^{-1/2} \\ &= \frac{1}{p+1} D_{p,v}^{-1/2} \left( \sum_{\sigma_p \in \mathcal{K}_p} G_{\sigma_p} \right) D_{p,v}^{-1/2}. \end{aligned} \quad (13)$$

We now consider the bilinear form of  $\mathcal{L}_p$ ,

$$\begin{aligned} y^\top \mathcal{L}_p y &= \frac{1}{p+1} \left( y^\top D_{p,v}^{-1/2} \right) \sum_{\sigma_p \in \mathcal{K}_p} G_{\sigma_p} \left( D_{p,v}^{-1/2} y \right) \\ &= \frac{1}{p+1} D_{p,v}^{-1/2} \sum_{\sigma_p \in \mathcal{K}_p} \left( x^\top G_{\sigma_p} x \right) D_{p,v}^{-1/2} \\ &\geq 0. \end{aligned} \quad (14)$$

Here,  $x = D_{p,v}^{-1/2} y$ . It follows that  $\mathcal{L}_p$  are positive semidefinite for arbitrary  $p$ . □

According to Lemma A.1 and Lemma A.2, it can be directly drawn that  $0 \leq \lambda(\tilde{\mathcal{A}}_p) = \lambda(I - \mathcal{L}_p) \leq 1$ . In a similar way, one can conclude that  $0 \leq \lambda(\mathcal{L}_p) \leq 1$ .

**Lemma A.3.** *0 is an eigenvalue of the higher-order flower-petals Laplacian matrices  $\mathcal{L}_p$ .*

*Proof.* Let  $\mathbf{1} = (1, 1, \dots, 1)^\top$  be an all-one vector. According to the definition of  $\mathcal{H}_p$ , we can obtain that  $\mathcal{H}_p^\top \mathbf{1} = (p+1)\mathbf{1}$  and  $\mathcal{H}_p \mathbf{1} = D_{p,v}$ . It follows that

$$\begin{aligned} \mathcal{L}_p \mathbf{1} &= \left( I - \frac{1}{p+1} D_{p,v}^{-1/2} \mathcal{H}_p \mathcal{H}_p^\top D_{p,v}^{-1/2} \right) \mathbf{1} \\ &= D_{p,v}^{-1/2} \left( D_{p,v} - \frac{1}{p+1} \mathcal{H}_p \mathcal{H}_p^\top \mathbf{1} \right) D_{p,v}^{-1/2} \\ &= 0. \end{aligned} \quad (15)$$

Therefore,  $\mathbf{1}$  is an eigenvector of  $\mathcal{L}_p$  associated with eigenvalue 0, which is also the smallest eigenvalue from the non-negativity of  $\mathcal{L}_p$ . □

## B Expressive power analysis details

### B.1 Introduction to the Weisfeiler-Lehman test

The Weisfeiler-Lehman (WL) graph isomorphism test (Weisfeiler and Leman 1968) provides a well-studied framework for the unique assignment of node labels. An intrinsic theoretical connection has been uncovered between the WL test and spatial GNNs (Xu et al. 2019; Morris et al. 2019). Here, we first present a brief introduction to the WL test.

---

#### Algorithm 1: Weisfeiler-Lehman Test

---

**Input:** Graph  $\mathcal{G}$ , initial node coloring  $\{c^{(0)}(v_1), c^{(0)}(v_2), \dots, c^{(0)}(v_n)\}$   
**Output:** Final node coloring  $\{c^{(T)}(v_1), c^{(T)}(v_2), \dots, c^{(T)}(v_n)\}$ .

```

1:  $t \leftarrow 0$ 
2: repeat
3:   for  $v$  in  $\mathcal{V}$  do
4:      $c^{(t+1)}(v) = \text{Hash}(\{\{c^{(t)}(u) | u \in N(v) \cup \{v\}\}\})$ 
5:   end for
6:    $t \leftarrow t + 1$ 
7: until stable node coloring is reached

```

---

Two graphs  $\mathcal{G}$  and  $\mathcal{G}'$  are considered to be isomorphic if there exists an edge-preserving bijection  $\psi : \mathcal{V} \rightarrow \mathcal{V}'$ , i.e.,

$(u, v) \in \mathcal{E}(\mathcal{G})$  if and only if  $(\psi(u), \psi(v)) \in \mathcal{E}(\mathcal{G}')$ . Graph isomorphism determination is an NP-hard problem, and the Weisfeiler-Lehman test, or  $k$ -WL, is a family of heuristic algorithms for testing graph isomorphism (Morris et al. 2019).  $k$ -WL constructs a coloring  $c$  of the tuples of  $k$  nodes, that is  $c : \mathcal{V}^k \rightarrow \Sigma$  with arbitrary codomain  $\Sigma$ .

We now describe the WL test for graph  $\mathcal{G}$  with coloring  $c$ . In each iteration  $t$ , the WL algorithm updates a new coloring according to the rule

$$c^{(t+1)}(v) = \text{Hash} \left( \left\{ \left\{ c^{(t)}(u) \mid u \in N(v) \cup \{v\} \right\} \right\} \right), \quad (16)$$

where  $\text{Hash}(\cdot)$  bijectively maps different multi-set inputs  $\{\cdot\}$  to a unique color in  $\Sigma$ , and  $N(v)$  presents the set of nodes adjacent to node  $v$  in  $\mathcal{G}$ , i.e.,  $N(v) = \{u \in \mathcal{V} \mid (v, u) \in \mathcal{E}\}$ . The iteration is finished until stable node coloring is reached, i.e.,  $c^{(t+1)} = c^{(t)}$ , and termination is guaranteed within  $\max\{|\mathcal{V}|, |\mathcal{E}|\}$  iterations.

To distinguish two graphs  $\mathcal{G}$  and  $\mathcal{G}'$  in terms of isomorphism, we perform the WL test on both  $\mathcal{G}$  and  $\mathcal{G}'$  in parallel, and these two graphs are non-isomorphic if their color histograms are different in the iteration.

The  $k$ -WL test ( $k \geq 2$ ) is a generalized version of the WL test that colors the tuples  $\mathcal{V}^k$  instead of  $\mathcal{V}$ . The algorithms with larger  $k$  are more powerful in distinguishing non-isomorphic graphs. However, it is noted that although the  $k$ -WL test is a powerful heuristic, it is not guaranteed to be effective in all cases (Cai, Fürer, and Immerman 1992). Without causing ambiguity, we abbreviate the 1-WL test as the WL test to unload the notation burden.

## B.2 Higher-order version of WL test

The proposed higher-order Weisfeiler-Lehman test, termed HWL, extends the WL test to simplicial complexes. SHWL, a simplified version of HWL, further reduces the coloring rule. We can relate the expressive power of HWL, SHWL and WL by clique complex lifting transition, and it has been found that both HWL and SHWL are more powerful than Weisfeiler-Lehman in terms of expressive power.

We outline below the steps of HWL in a given simplicial complex  $\mathcal{K}$  for example.

(a) Assign the same initial color  $c^{(0)}(\sigma)$  to each simplex  $\sigma$  in  $\mathcal{K}$ .

(b) Given the color  $c^{(t)}(\sigma)$  of simplex  $\sigma$  at the  $t$ -th iteration. We will refine its color by injectively mapping neighborhood colors in the flower-petals model according to

$$c^{(t+1)}(\sigma) = \text{Hash} \left( c^{(t)}(\sigma), \left\{ \left\{ c^{(t)}(\tau) \mid \tau \in \mathcal{N}(\sigma) \right\} \right\} \right). \quad (17)$$

Here, the Hash function maps different multi-set inputs to different colors,  $\mathcal{N}(\sigma) = \bigcup_p \mathcal{N}_p(\sigma)$ , and  $\mathcal{N}_p$  denotes the set of neighbors of  $\sigma$  in the bipartite graph  $\mathcal{G}_p$ .

(c) The algorithm stops until a stable coloring is reached. Two simplicial complexes are considered non-isomorphic if their color histograms are different at any iteration. Otherwise, the test is inconclusive.

**Theorem B.1.** *HWL with clique complex lifting is strictly more powerful than Weisfeiler-Lehman (WL) test.*

The proof is deferred to Appendix B.3.

Moreover, we can simplify the coloring rule for simplices whose order is larger than zero to nonvanishing linear functions, i.e.,

$$c^{(t+1)}(\sigma) = \text{Linear} \left( c^{(t)}(\sigma), \left\{ \left\{ c^{(t)}(\tau) \mid \tau \in \mathcal{N}(\sigma) \right\} \right\} \right). \quad (18)$$

Here,  $\dim(\sigma) > 0$  and  $\text{Linear}(\cdot)$  is a nonvanishing linear function requiring that the coefficients of the polynomial never be zero. Other steps are the same as in HWL, and the simplified version of HWL, referred to as SHWL, is shown in Algorithm 2.

We find that SHWL is still more powerful than the WL test (refer to Theorem 4.2).

---

### Algorithm 2: Simplified Higher-order WL Test (SHWL)

---

**Input:** Simplicial complex  $\mathcal{K}$ , initial simplicial coloring  $\{c^{(0)}(\sigma_1), c^{(0)}(\sigma_2), \dots\}$

**Output:** Final node coloring  $\{c^{(T)}(v_1), \dots, c^{(T)}(v_n)\}$ .

```

1:  $t \leftarrow 0$ 
2: repeat
3:   for  $v$  in  $\mathcal{V}$  do
4:      $c^{(t+1)}(v) = \text{Hash} \left( c^{(t)}(v), \left\{ \left\{ c^{(t)}(\tau) \mid \tau \in \mathcal{N}(v) \right\} \right\} \right)$ 
5:   end for
6:   for  $\sigma$  in  $\mathcal{K}_1 \cup \mathcal{K}_2 \cup \dots$  do
7:      $c^{(t+1)}(\sigma) = \text{Linear} \left( c^{(t)}(\sigma), \left\{ \left\{ c^{(t)}(v) \mid v \in \mathcal{N}(\sigma) \right\} \right\} \right)$ 
8:   end for
9:    $t \leftarrow t + 1$ 
10: until stable simplicial coloring is reached

```

---

In dense graphs, the number of total simplices is much larger than the node number. It is not necessary to explicitly figure out messages for higher-order structures when tackling the most common node-level tasks. Hence, we can perform the two message-passing steps simultaneously. By replacing the colors with continuous feature vectors in the SHWL test and replacing the Hash function with a neural network layer-like differentiable function with learnable parameters, we can obtain

$$X^{(k+1)} = \sigma \left( \tilde{\mathcal{A}}_p X^{(k)} \Theta_p^{(k)} \right). \quad (19)$$

Here,  $X^{(k)} \in \mathbb{R}^{n \times d}$  is the signal at the  $k$ -th layer,  $X^{(0)} = X$  presents the initial node features, and  $\sigma(\cdot)$  is differentiable non-linear transition function. Following (Wu et al. 2019), the non-linear transition functions between the layers are removed. Besides, by linearly combining the results from different layers, we can further obtain that

$$Y_p = \sum_{k=0}^K \gamma_{p,k} \tilde{\mathcal{A}}_p^k X \Theta_p. \quad (20)$$

Here,  $\Theta_p = \Theta_p^{(1)} \Theta_p^{(2)} \dots \Theta_p^{(K)}$  is reparameterized.

We finally concatenate the results from different FP convolutions followed by a linear layer to reshape the output as follows

$$Y = \prod_{p=1}^P \left( \sum_{k=0}^K \gamma_{p,k} \tilde{\mathcal{A}}_p^k X \Theta_p \right) W. \quad (21)$$

Therefore, the HiGCN model can be interpreted as a neural version of the SHWL test. Theorem 4.2 suggests that the proposed HiGCN model endows with greater potential than the traditional GNNs.

### B.3 Proofs of HWL and SHWL theory

We begin by introducing some required notions and symbols. Note that although these results apply mainly to simplicial complexes, they also work for graphs since graphs can be viewed as special simplicial complexes. Besides, we can also obtain a unique simplex complex by taking clique complex lifting.

**Definition B.2.** A simplicial coloring  $c$  is a mapping that assigns a color from a specific color scheme to a simplicial complex  $\mathcal{K}$  and its simplices  $\sigma$ . We denote this color as  $c^{\mathcal{K}}(\sigma)$ , or as  $c(\sigma)$  when it does not cause ambiguity.

**Definition B.3.** Let  $c$  be a simplicial coloring. Simplicial complexes  $\mathcal{J}, \mathcal{K}$  are considered to be  $c$ -similar, represented by  $c^{\mathcal{J}} = c^{\mathcal{K}}$ , if the numbers of simplices with the same color in  $\mathcal{J}$  and  $\mathcal{K}$  are identical. Otherwise, we say  $c^{\mathcal{J}} \neq c^{\mathcal{K}}$ .

**Definition B.4.** A simplicial coloring  $c$  refines another one  $d$ , noted as  $c \sqsubseteq d$ . Then for all simplicial complexes  $\mathcal{J}, \mathcal{K}$  and all  $\sigma \in \mathcal{J}, \tau \in \mathcal{K}$ ,  $d^{\mathcal{J}}(\sigma) = d^{\mathcal{K}}(\tau)$  iff  $c^{\mathcal{J}}(\sigma) = c^{\mathcal{K}}(\tau)$ .

If  $d^{\mathcal{J}}(\sigma) \neq d^{\mathcal{K}}(\tau)$  for two simplicial colorings  $c$  and  $d$  satisfying the relation  $c \sqsubseteq d$ , then we can obtain  $c^{\mathcal{J}}(\sigma) \neq c^{\mathcal{K}}(\tau)$  (Bodnar et al. 2021). This conclusion implies that if  $c$  refines  $d$ , then  $c$  is capable of distinguishing all non-isomorphic simplicial complex pairs that  $d$  can distinguish. In this sense, we consider  $c$  to be at least as powerful as  $d$ .

Equipped with this background knowledge, we are now set up to prove the conclusions in the main article. To begin with, we introduce a slightly weak version of Theorem B.1.

**Lemma B.5.** *HWL is at least as powerful as Weisfeiler-Lehman (WL) test in distinguishing non-isomorphic simplicial complexes.*

*Proof.* Let notion  $a^{(t)}$  denote the coloring of the Weisfeiler-Lehman test with the coloring update rule  $a^{(t+1)}(v) = \text{Hash}(a^{(t)}(v), \{\{a^{(t)}(u) | u \in N(v)\}\})$  and  $c^{(t)}$  the coloring of HWL test for the same nodes in  $\mathcal{K}$  using the rule  $c^{(t+1)} = \text{Hash}(c^{(t)}(\sigma), \{\{c^{(t)}(\tau) | \tau \in \mathcal{N}(\sigma)\}\})$ . Note that the function  $\text{Hash}(a^{(t)}(v), \{\{a^{(t)}(u) | u \in N(v)\}\})$  and  $\text{Hash}(\{\{a^{(t)}(u) | u \in N(v) \cup \{v\}\}\})$  are equivalent.

We additionally introduce  $b^{(t)}$  to represent the coloring of restricted HWL that utilizes information no larger than 1-simplex, i.e., the refine rule can be represented as  $b^{(t+1)}(\sigma) = \text{Hash}(b^{(t)}(\sigma), \{\{b^{(t)}(\tau) | \tau \in \mathcal{N}_1(\sigma)\}\})$ . Here,  $\mathcal{N}_1(\sigma)$  denotes the set of neighbours of  $\sigma$  in the bipartite graph  $\mathcal{G}_1$ . It's trivial to show  $c$  refines  $b$  since it considers the additional colors from higher-order simplices. We now only have to prove that  $b^{(2t)} \sqsubseteq a^{(t)}$  by induction.

The base case holds for all colors are the same at initialization. For the induction step, suppose it satisfies  $b^{(2t+2)}(v) = b^{(2t+2)}(u)$  for any two 0-simplices  $v$  and  $u$  in two arbitrary complexes. The inputs to the Hash function need to be the same as the SWL coloring is an injective

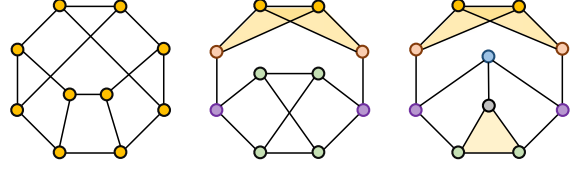


Figure 4: Three non-isomorphic graphs that are indistinguishable by WL but distinguishable by HWL and SHWL with clique complex lifting. The incorporation of higher-order information in HWL and SHWL enables nodes to exhibit a more extensive diversity in color compared to the WL test, consequently yielding superior performance in both node-level and graph-level tasks.

mapping. Hence, we can obtain  $b^{(2t+1)}(v) = b^{(2t+1)}(u)$  and  $\{\{b^{(2t+1)}(\sigma) | \sigma \in \mathcal{N}_1(v)\}\} = \{\{b^{(2t+1)}(\tau) | \tau \in \mathcal{N}_1(u)\}\}$ . By unwrapping the hash function, we can get

$$\begin{aligned} b^{(2t+1)}(\sigma) &= \text{Hash}\left(b^{(2t)}(\sigma), \{\{b^{(2t)}(w) | w \in \mathcal{N}_1(\sigma)\}\}\right) \\ &= \text{Hash}\left(b^{(2t)}(\sigma), \{\{b^{(2t)}(w) | w \in N(v) \cup \{v\}\}\}\right). \end{aligned} \quad (22)$$

Similarly, we can obtain

$$b^{(2t+1)}(\tau) = \text{Hash}\left(b^{(2t)}(\tau), \{\{b^{(2t)}(w) | w \in N(u) \cup \{u\}\}\}\right). \quad (23)$$

By removing the same color  $b^{(2t)}(\sigma)$  and  $b^{(2t)}(\tau)$  from the input, we can further obtain that  $\{\{b^{(2t)}(w) | w \in N(v) \cup \{v\}\}\} = \{\{b^{(2t)}(w) | w \in N(u) \cup \{u\}\}\}$ . According to the induction hypothesis  $b^{(2t)} \sqsubseteq a^{(t)}$ , it can be deduced that  $\{\{a^{(t)}(w) | w \in N(v) \cup \{v\}\}\} = \{\{a^{(t)}(w) | w \in N(u) \cup \{u\}\}\}$ . We can finally conclude that  $a^{(t+1)}(v) = a^{(t+1)}(u)$ , which implies  $b^{(2t+2)} \sqsubseteq a^{(t+1)}$ .  $\square$

**Proof of Theorem B.1.** In accordance with Lemma B.5, we only need to provide a pair of non-isomorphic graphs that WL fails to distinguish, while HWL can distinguish with the assistance of a clique complex lifting transition. Any two graphs in Figure 4 constitute such a pair that satisfies these criteria.  $\square$

Moreover, we can simplify the coloring rule for simplices whose order is larger than 0 to nonvanishing linear functions, resulting in a simplified version of HWL, termed SHWL. The nonvanishing linear function implies that the polynomial coefficient will never be 0. We will demonstrate that the SHWL test remains more powerful than the WL test.

**Lemma B.6.** *SHWL is at least as powerful as Weisfeiler-Lehman (WL) test in distinguishing non-isomorphic simplicial complexes.*

*Proof.* Let notion  $a^{(t)}$  denote the coloring of WL test with the rule  $a^{(t+1)}(v) = \text{Hash}(a^{(t)}(v), \{\{a^{(t)}(u)|u \in N(v)\}\})$  and  $c^{(t)}$  the coloring of SHWL for the same nodes in  $\mathcal{K}$  using  $c^{(t+1)} = \text{Hash}(c^{(t)}(\sigma), \{\{c^{(t)}(\tau)|\tau \in \mathcal{N}(\sigma)\}\})$ .

We additionally introduce  $b^{(t)}$  to represent the coloring of restricted SHWL that utilizes information no larger than 1-simplex, i.e. the refine rule can be represented as  $b^{(t+1)}(\sigma) = \text{Hash}(b^{(t)}(\sigma), \{\{b^{(t)}(\tau)|\tau \in \mathcal{N}_1(\sigma)\}\})$ . Here,  $\mathcal{N}_1(\sigma)$  denotes the set of neighbours of  $\sigma$  in the bipartite graph  $\mathcal{G}_1$ . It's trivial to show  $c \sqsubseteq b$  since it considers the additional colors from higher-order simplices. We now only have to prove that  $b^{(2t)} \sqsubseteq a^{(t)}$  by induction.

The base case holds for all colors are the same at initialization. For the induction step, suppose it satisfies  $b^{(2t+2)}(v) = b^{(2t+2)}(u)$  for any two 0-simplices  $v$  and  $u$  in two arbitrary complexes. Then we can obtain  $b^{(2t+1)}(v) = b^{(2t+1)}(u)$  and  $\{\{b^{(2t+1)}(\sigma)|\sigma \in \mathcal{N}_1(v)\}\} = \{\{b^{(2t+1)}(\tau)|\tau \in \mathcal{N}_1(u)\}\}$ , since these are the arguments of the hash function. By unwrapping the coloring rule, we can obtain

$$\begin{aligned} b^{(2t+1)}(\sigma) &= \text{Linear}\left(b^{(2t)}(\sigma), \{\{b^{(2t)}(w)|w \in \mathcal{N}_1(\sigma)\}\}\right) \\ &= \text{Linear}\left(b^{(2t)}(\sigma), \{\{b^{(2t)}(v), b^{(2t)}(w)|w \in N(v)\}\}\right) \\ &= \text{Linear}\left(\{\{b^{(2t)}(w)|w \in N(v) \cup \{v, \sigma\}\}\}\right). \end{aligned} \quad (24)$$

Similarly, we can obtain

$$b^{(2t+1)}(\tau) = \text{Linear}\left(\{\{b^{(2t)}(w)|w \in N(u) \cup \{u, \tau\}\}\}\right). \quad (25)$$

Since the coloring  $b^{(2t)}(\sigma)$  and  $b^{(2t)}(\tau)$  are the same, we can further obtain  $\text{Linear}(\{\{b^{(2t)}(w)|w \in N(v) \cup \{v\}\}\}) = \text{Linear}(\{\{b^{(2t)}(w)|w \in N(u) \cup \{u\}\}\})$  by removing the same color from the linear function. Because the linear function is nonvanishing, we can finally conclude that  $a^{(t+1)}(v) = a^{(t+1)}(u)$ , which implies  $b^{(2t+2)} \sqsubseteq a^{(t+1)}$ .  $\square$

**Proof of Theorem 4.2.** According to Lemma B.6, we only have to offer a pair of non-isomorphic graphs that WL fails to distinguish, while SHWL can distinguish with the help of clique complex lifting transition. It might as well to assume the nonvanishing linear function to be a summation function, and such a non-isomorphic graph pair is demonstrated in Figure 4.  $\square$

## C Relation to other GCN models

If we consider only the information transfer process based on the edge (1-simplex) in the bipartite graph  $\mathcal{G}_1$ , then the higher-order FP adjacency matrix can be represented as:

$$\tilde{\mathcal{A}}_1 = \frac{1}{2}D^{-1/2}\mathcal{H}_1\mathcal{H}_1^\top D^{-1/2} = \frac{1}{2}\left(D^{-1/2}AD^{-1/2} + I\right). \quad (26)$$

Here, we omit the subscript for  $D_{1,v}$  to unload the notation, for it retains the same meaning as in pairwise graphs without causing ambiguity. It can be drawn that the definition of FP adjacency matrices preserves the topological feature of the original graph. Additionally, there is no need to add self-loops since they are already implicitly included in the FP adjacency matrices. Therefore, HiGCN can be viewed as an extension of vanilla spatial GNNs within the higher-order domain.

In particular, GPRGNN (Chien et al. 2020), one of the state-of-the-art spectral GNNs related to HiGCN, can be considered a special case of HiGCN if we only account for information interactions between 0-simplices and 1-simplices, i.e., requiring parameter  $P = 1$ . Moreover, GCN (Kipf and Welling 2017) also constitutes a specific instance of our model if we employ a fixed low-pass filter and fix  $P = 1$ .

On the other hand, HiGCN demonstrates enhanced flexibility over certain Hodge Laplacian-based simplicial GCNs, transcending the constraints imposed by information exchange exclusively through boundary operators. Specifically, HiGCN generalizes simplicial convolution operations on simplicial complexes, encompassing SNN (Ebli, Defferard, and Spreemann 2020) and SCNN (Yang, Isufi, and Leus 2022), if we apply fixed low-pass filters and require  $P = 1$  for node-level tasks.

## D Random walk model

Graph neural networks can also be interpreted as a modified random walk of information over graph structures (Gasteiger, Bojchevski, and Günnemann 2019). The main idea of random walks is to traverse a graph starting from a single node or a set of nodes and get sequences of locations (Zeng et al. 2023).

In unbiased random walk models, suppose a random walker is located at node  $i$  and he will wander to a neighbouring vertex  $j$  with probability  $A_{ij}/k_j$ , reflecting an equal selection between  $k_j$  neighbours. In mathematical, this process can be formulated as

$$\pi_i(t) = \sum_j \frac{A_{ij}}{k_j} \pi_j(t-1). \quad (27)$$

Here,  $k_j$  stands for the degree of node  $j$ . It can be expressed equivalently as

$$\pi(t) = AD^{-1}\pi(t-1), \quad (28)$$

where  $\pi(t) = (\pi_1(t), \dots, \pi_n(t))^\top$  and  $D = \text{diag}(k_1, \dots, k_n)$ .

Multiplying  $D^{-1/2}$  from left sides of the equation (28) simultaneously, we can obtain

$$D^{-1/2}\pi(t) = \left[D^{-1/2}AD^{-1/2}\right] D^{-1/2}\pi(t-1). \quad (29)$$

Here,  $D^{-1/2}AD^{-1/2}$  is a symmetric matrix and is referred to as a reduced adjacency matrix. Based on the reduced adjacency matrix, we can obtain the normalized graph Laplacian

$$L = I - D^{-1/2}AD^{-1/2}. \quad (30)$$



## E Equivariance and invariance

Equivariance and invariance are fundamental concepts in understanding GNNs and their behavior when processing graph-structured data. In accordance with recent endeavors in simplicial neural networks to examine various models in terms of equivariance (Bodnar et al. 2021; Qu, Huang, and Zheng 2020; Yang, Isufi, and Leus 2022), our objective herein is to elucidate the fundamental equivariance properties intrinsic to the HiGCN model.

Consider a simplicial complex  $\mathcal{K}$  with a maximum simplex order of  $\ell$  and a sequence  $\mathbf{H} = (\mathcal{H}_1, \dots, \mathcal{H}_\ell)$  of higher-order incidence matrices. Let  $\mathbf{P} = (P, P_1, \dots, P_\ell)$  represent a sequence of simplicial permutation matrices with  $P \in \mathbb{R}^{n \times n}$  and  $P_i \in \mathbb{R}^{n_i \times n_i}$ . Denote the permutation features as  $PX$  and the sequence of permutation higher-order incidence matrices  $(PH_1P_1, \dots, PH_\ell P_\ell)$  as  $\mathbf{PHP}^\top$ .

**Definition E.1.** A function  $f$  is simplex permutation equivariant if  $f(PX, \mathbf{PHP}^\top) = Pf(X, \mathbf{H})$  for any sequence of permutation operators  $\mathbf{P}$ .

**Theorem E.2.** The HiGCN model is simplex permutation equivariant.

*Proof.* After a sequence of permutations  $\mathbf{P}$ , the higher-order incidence matrix  $\mathcal{H}_p$  is transformed into  $P\mathcal{H}_pP_p^\top$  and  $D_{p,v}$  becomes  $PD_{p,v}P^\top$ . Consequently, the permuted FP adjacency matrix  $\tilde{\mathcal{A}}_p$  is given by

$$\begin{aligned} \tilde{\mathcal{A}}_p' &= \frac{1}{p+1} D_{p,v}'^{-1/2} \mathcal{H}_p' \mathcal{H}_p'^\top D_{p,v}'^{-1/2} \\ &= \frac{1}{p+1} (PD_{p,v}^{-1/2} P^\top) (P\mathcal{H}_p P_p^\top) (P_p \mathcal{H}_p^\top P^\top) \\ &\quad (PD_{p,v}^{-1/2} P^\top) \\ &= \frac{1}{p+1} PD_{p,v}^{-1/2} \mathcal{H}_p \mathcal{H}_p^\top D_{p,v}^{-1/2} P^\top \\ &= P\tilde{\mathcal{A}}_p P^\top. \end{aligned} \quad (31)$$

Therefore, we can deduce  $\tilde{\mathcal{A}}_p'^k = P\tilde{\mathcal{A}}_p^k P^\top$ . Subsequently, we can express the permuted convolution output as

$$Y' = \left\| \left( \sum_{k=0}^K \gamma_{p,k} P\tilde{\mathcal{A}}_p^k P^\top PX \Theta_p \right) W \right\| = PY. \quad (32)$$

Moreover, as the employed non-linear activation function and readout function exhibit equivariance, the HiGCN model is simplex permutation equivariant.  $\square$

Comprehending equivariance and invariance in GNNs is of paramount importance for devising effective models and training methodologies. By taking these properties into account, GNN architectures can be developed to capitalize on equivariance in order to capture and propagate local structural information, while simultaneously ensuring invariance to concentrate on graph-level or task-specific features.

## F Experimental details for quantification of higher-order interaction strengths

### F.1 Construction of 1k null model

The null model (Orsini et al. 2015) refers to a class of random networks endowing with some of the same properties as an actual network, and they are often employed to quantify the extent of some special properties. The 1k null model (Yang et al. 2023) is the network that has the same node number and edge number as the origin network. The construction of the 1k null model with a changeable triangle number is divided into two parts: (1) node-picking and (2) relinking.

In the node-picking process, we traverse all nodes in the graph and find node A with more than two neighbors. Based on node A, we pick two neighbor nodes node B and node C which are not connected. We then pick neighbor nodes D and E of node B and node C, which should not be connected with node A. Notice that nodes D and E can not connect with each other, so the whole chain of D-B-A-C-E contains no triangle.

In the relinking step, we break the original edges  $[B, D]$  and  $[C, E]$ , and then add edges  $[B, C]$  and  $[D, E]$  (red edges in Figure 5). In this way, a new triangle  $[A, B, C]$  (gray shade in Figure 5) is added with the number of nodes and edges stable.

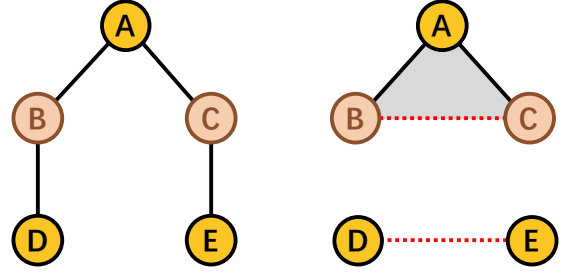


Figure 5: **The modification process of the 1k null model.** The left and right figures show the partial structures of the networks before and after modification, respectively.

### F.2 More experimental results

HiGCN achieves the optimal results in node classification tasks except for Texas, see Table 2. It has also been noticed in Figure 3(d) that Texas's higher-order interactions are pretty weak compared to its lower-order ones, along with the least triangles over all datasets (see Table 9). Therefore, few higher-order structures may lead to weak higher-order influence, along with degraded node classification performance of HiGCN. To verify this conjecture, we modify the number of higher-order structures by adjusting the connectivity of edges in the network while maintaining the degree distribution as in 1k null models. Table 5 shows the node classification results under different relative triangle densities from 0 (original network) to +50% in units of 10%. An increasing accuracy rank is observed between HiGCN and the benchmark with the rise of the triangles' density  $\rho_2$ . In

particular, HiGCN performs best at higher relative triangle densities  $\rho_2 = 20\%$ ,  $40\%$ , and  $50\%$ .

As for the Actor dataset, where HiGCN has already achieved the best-ranking performance, Table 6 shows the node classification results under different relative triangle densities from 0 (original network) to +50% in units of 10%. An increasing leading superiority is observed between HiGCN and the rank-2 method with the rise of the triangles' density  $\rho_2$ .

The process of constructing a 1k null model can also be considered as adding specific noise to the network, and it can be found from Table 5 and Table 6 that our model excels in handling noise containing higher-order information.

Figure 6 indicates the sum of  $\gamma_{2,k}$ 's absolute value under the relative triangle densities (from  $-50\%$  to  $+50\%$  in units of 10%), which represents the influence of higher-order structures.

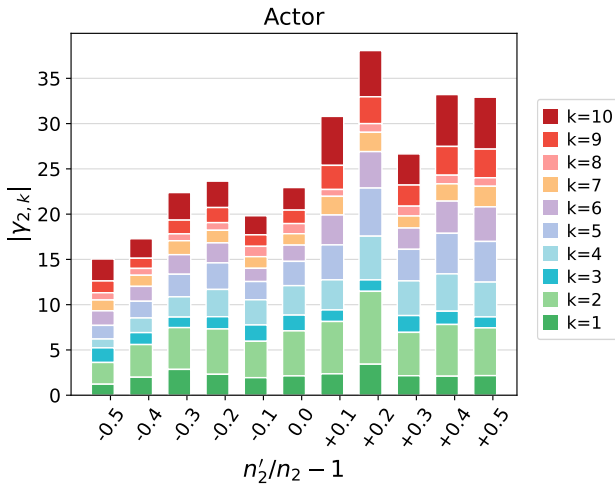


Figure 6: The stack of the learned weights  $|\gamma_{2,k}|$  for Actor with different relative triangle density  $\rho_2 = n'_2/n_2 - 1$ .

### F.3 Sensitivity to the parameter initialization

We initialize the graph filter weights as  $\gamma_{p,k} = \alpha(1 - \alpha)^k$  and  $\gamma_{p,K} = (1 - \alpha)^K$  following (Gasteiger, Bojchevski, and Günnemann 2019), where  $\alpha$  is hyperparameter. A series of experiments are conducted to scrutinize the sensitivity of our model to parameter initialization by considering various  $\alpha$  values within the range  $\{0.1, 0.2, \dots, 0.9\}$ . Specifically, we visualize the variations in  $\gamma$  as the training steps progress for distinct initializations of  $\alpha$  in Figure 7. The results demonstrate that all different initial values eventually converge to a stable value as the training step increases. Consequently, we can conclude that the higher-order interaction strength  $S_p = \sum |\gamma_{p,k}|$  and the performance of our model are not reliant on the choice of the initial value.

## G Experiments on large-scale datasets and computational analysis

We additionally conduct experiments on three larger datasets: two homogeneous graphs (Ogbn-arxiv (Hu et al.

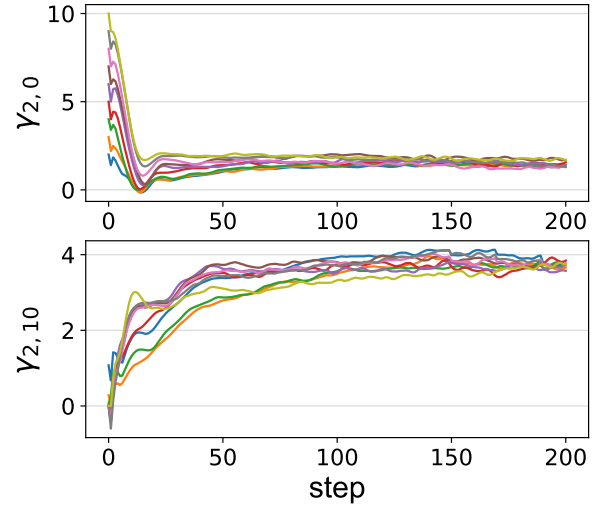


Figure 7: Training dynamics of  $\gamma$  under various initializations.

2020) and Genius (Lim and Benson 2021)) and one heterogeneous graph (Penn94 (Traud, Mucha, and Porter 2012)). The results in Table 7 demonstrate that our HiGCN model outperforms other methods in the node classification task while maintaining a reasonable computational cost.

We also examine the computational complexity of HiGCN compared to other node classification baselines and report the average training time per epoch and average total running time in Table 8.

Moreover, when the targeted graph is not in the form of SCs, one should also consider the one-time preprocessing procedure for graph lifting. Specifically, the number of  $p$ -simplices in a graph with  $n$  nodes and  $m$  edges is upper-bounded by  $\mathcal{O}(n^{p-1})$ , and they can be enumerated in  $\mathcal{O}(a(\mathcal{G})^{p-3}m)$  time (Chiba and Nishizeki 1985), where  $a(\mathcal{G})$  is the arboricity of the graph  $\mathcal{G}$ , a measure of graph sparsity. Since arboricity is demonstrated to be at most  $\mathcal{O}(m^{1/2})$  and  $m \leq n^2$ , all  $p$ -simplices can thus be listed in  $\mathcal{O}(n^{p-3}m)$ . Besides, the complexity of finding 2-simplex is estimated to be  $\mathcal{O}(\langle k \rangle m)$  with the Bron-Kerbosch algorithm (Bron and Kerbosch 1973), where  $\langle k \rangle$  denotes the average node degree, typically a small value for empirical networks.

## H Datasets

**Node classification.** Table 9 provides the statistics of all the datasets used in the node classification experiments. The homophily level of  $\mathcal{G}$  is measured by  $Homophily(\mathcal{G}) = \frac{|\{(u,v):(u,v) \in \mathcal{E} \wedge y_v = y_u\}|}{n_1}$  (Zhu et al. 2020), where  $y_v$  is the label of nodes  $v$  and  $n_1 = |\mathcal{E}|$  denotes the number of edges.

We additionally scale HiGCN to three large-scale datasets: Penn94, Ogbn-arxiv, and Genius. **Penn94** (Traud, Mucha, and Porter 2012) is a social network extracted from Facebook where nodes represent students and edges denote the communication relationship of students. **Ogbn-arxiv** (Hu et al. 2020) is a paper citation network of arxiv pa-

$\rho_2$	0	10%	20%	30%	40%	50%
MLP	91.45±1.14	91.02±0.98	91.90±0.95	91.18±1.11	91.74±0.92	91.05±0.95
GCN	75.16±0.96	64.36±1.83	64.89±2.16	64.07±1.93	62.92±2.34	64.75±2.16
GAT	78.87±0.86	79.97±1.03	78.89±1.07	78.20±1.20	77.28±1.30	77.93±1.42
ChebNet	86.08±0.96	82.10±1.52	83.08±1.09	79.21±1.55	81.34±1.48	81.41±1.34
BernNet	<b>93.12±0.65</b>	<b>92.10±0.95</b>	92.89±0.92	<b>92.33±1.08</b>	91.54±1.02	91.57±1.21
GGCN	85.81±1.72	85.95±1.42	85.51±1.67	83.84±1.70	91.15±1.02	83.95±1.73
APPNP	90.98±1.64	89.87±1.01	89.31±1.05	89.08±0.98	90.39±1.10	89.57±1.10
GPRGNN	92.95±1.30	86.10±2.76	88.16±1.13	83.05±2.05	84.69±1.77	83.54±2.72
<b>HiGCN</b>	92.45±0.73	91.70±1.06	<b>93.11±0.87</b>	91.64±1.14	<b>91.93±0.84</b>	<b>92.24±1.41</b>
Rank	3	2	<b>1</b>	2	<b>1</b>	<b>1</b>

Table 5: Node classification results on Texas with changeable higher-order densities: mean accuracy (%)  $\pm$  95% confidence interval. Bold values indicate the best result.

$\rho_2$	0	10%	20%	30%	40%	50%
MLP	40.19±0.56	39.23±1.07	39.20±1.08	39.80±1.10	39.22±1.07	39.06±1.06
GCN	30.59±0.23	31.45±0.22	31.21±0.22	31.27±0.25	30.91±0.26	31.07±0.26
GAT	35.98±0.23	32.47±0.37	32.79±0.39	32.53±0.40	32.45±0.36	32.35±0.33
ChebNet	38.02±0.23	36.57±0.20	36.73±0.20	36.65±0.23	36.92±0.23	36.65±0.22
BernNet	41.79±1.91	40.47±1.51	40.17±1.66	40.37±1.65	40.23±1.68	40.32±1.67
GGCN	38.09±0.88	38.05±1.25	38.18±1.01	38.05±1.10	38.16±1.15	38.19±1.02
APPNP	39.66±0.55	38.18±1.23	38.44±1.05	38.36±1.08	38.47±1.19	38.26±1.12
GPRGNN	39.92±0.67	39.00±1.07	38.83±1.02	39.07±1.23	38.99±1.22	39.29±1.21
<b>HiGCN</b>	<b>41.81±0.52</b>	<b>41.28±0.34</b>	<b>41.47±0.29</b>	<b>41.15±0.28</b>	<b>41.46±0.31</b>	<b>41.57±0.30</b>
Increase	+0.02	+0.81	+1.30	+0.78	+1.23	+1.25

Table 6: Node classification results on Actor with changeable higher-order densities: mean accuracy (%)  $\pm$  95% confidence interval. Bold values indicate the best result.

Method	Penn94	Ogbn-arxiv	Genius
MLP	73.61±0.40	69.88±0.27	86.68±0.09
GCN	82.47±0.27	71.49±0.30	87.42±0.37
GAT	81.53±0.55	71.59±0.38	55.80±0.87
S2V	80.60±0.22	68.87±0.12	83.21±0.34
ChebNet	81.21±0.32	71.12±0.22	85.69±0.75
GPRGNN	81.38±0.16	71.78±0.18	90.09±0.31
ACM-GCN++	<b>86.08±0.43</b>	N/A	91.40±0.07
GloGNN++	<u>85.74±0.42</u>	N/A	90.91±0.13
DRGCN	N/A	<u>76.11±0.09</u>	N/A
LGGNN	N/A	75.70±0.18	N/A
1-HiGCN	83.01±0.44	73.86±0.25	89.98±0.73
2-HiGCN	85.66±0.59	76.00±0.41	91.53±0.36
3-HiGCN	85.68±0.67	<b>76.41±0.53</b>	91.60±0.61
4-HiGCN	84.98±0.32	76.01±0.38	<b>91.66±0.43</b>

Table 7: Node classification results on large-scale networks: mean accuracy (%)  $\pm$  95% confidence interval. The best results are in bold, while the second-best ones are underlined.

pers extracted from the Microsoft Academic Graph (MAG) where the nodes denote the papers and the edges denote the citation relationship. **Genius** (Lim and Benson 2021) is a

social network extracted from a website for crowdsourced annotations of song lyrics named “genius.com”. The nodes and edges of it represent users and the following relationship of users.

**Simplicial data imputation.** We extract three coauthorship complexes from DBLP (Benson et al. 2018), History and Geology (Sinha et al. 2015). In these coauthorship complexes, a paper with  $p + 1$  authors is represented by a  $p$ -simplex, and the  $p$ -simplicial signal corresponds to the number of collaborative publications among these authors. To mitigate the potential noise introduced by incidental collaborations, we consider coauthor groups with more than two collaborative publications as simplices. Following the standard pipeline for this task (Ebli, Defferrard, and Spreemann 2020), missing values are artificially introduced by replacing a portion of the signals with a constant. Table 10 provides the statistics of the coauthorship complexes that are employed.

**Graph classification.** In this study, we investigate various datasets from diverse domains to evaluate the performance of the proposed framework. The datasets are divided into two main categories: bioinformatics datasets and social network datasets.

The bioinformatics datasets comprise MUTAG, PTC, and

Dataset	2-HiGCN	3-HiGCN	4-HiGCN	APPNP	BERNNET	GPRGNN	CHEBNET	GGCN
Cora	2.8 / 0.6	3.0 / 0.7	3.3 / 0.9	3.6 / 1.2	11.6 / 3.1	4.3 / 0.9	4.6/2.2	5.2/2.4
Citeseer	3.0 / 0.7	3.2 / 0.7	3.4 / 0.9	3.7 / 1.3	11.8 / 3.4	4.5 / 1.0	5.4/2.4	2.4/2.7
Pubmed	4.8 / 1.0	5.7 / 1.2	6.3 / 1.3	3.9 / 2.0	11.1 / 4.9	4.5 / 1.8	6.0/3.0	7.2/7.3
Computers	6.2 / 1.3	6.5 / 1.4	7.0 / 1.6	6.0 / 2.5	29.3 / 8.6	6.5 / 1.6	21.1/12.7	18.3/15.1
Photo	5.3 / 1.1	5.6 / 1.2	6.3 / 1.3	5.8 / 2.8	15.3 / 6.2	4.5 / 1.3	19.8/11.9	19.0/10.3
Chameleon	4.4 / 1.3	4.8 / 1.5	5.3 / 1.6	3.9 / 0.8	11.0 / 2.8	4.4 / 1.0	5.0/2.3	4.8/5.2
Actor	2.7 / 0.8	3.1 / 0.9	3.5 / 1.1	3.8 / 0.8	10.9 / 3.5	4.3 / 0.9	4.2/1.8	4.7/4.9
Squirrel	8.5 / 2.6	8.9 / 2.8	9.6 / 3.0	4.3 / 0.9	15.7 / 4.9	4.3 / 2.1	6.3/3.5	11.4/14.7
Texas	2.4 / 0.7	2.6 / 0.8	2.8 / 0.8	3.8 / 0.8	11.3 / 2.4	4.3 / 1.0	2.5/0.9	2.1/1.5
Wisconsin	2.5 / 0.7	3.0 / 0.9	3.2 / 1.0	3.9 / 0.8	11.0 / 2.6	4.4 / 0.9	2.6/1.0	2.6/1.9

Table 8: Efficiency on node classification experiments: Average running time per epoch(ms)/ average total running time(s).

Network	Classes	Features	Homophily	$n$	$n_1$	$n_2$	$\langle k \rangle$
Cora	7	1433	0.8099	2708	5278	1630	3.90
Citeseer	6	3703	0.7355	3327	4552	1167	2.74
PubMed	5	500	0.8023	19717	44324	12520	4.50
Computers	10	767	0.7772	13752	245861	1527469	35.76
Photo	8	745	0.8272	7650	119081	717400	31.13
Chameleon	5	2325	0.2305	2277	31421	343066	27.60
Actor	5	2089	0.2187	7600	26659	7121	7.02
Squirrel	5	932	0.2224	5201	198493	9595609	76.33
Texas	5	1703	0.0871	183	279	67	3.05
Wisconsin	5	1703	0.1921	251	450	118	3.56
Penn94	2	5	0.470	41554	1362229	7207796	65.6
Ogbn-arxiv	40	128	0.655	169343	1157799	2233524	13.7
Genius	2	12	0.618	421961	984979	1968352	4.7

Table 9: Statistics of node classification datasets.

**PROTEINS**. **MUTAG** (Debnath et al. 1991) comprises 188 mutagenic aromatic and heteroaromatic nitro compounds with seven discrete labels. The goal is to identify mutagenic molecular compounds for potential drug development. **PTC** (Toivonen et al. 2003) involves classifying graph-structured compounds based on their carcinogenic properties in rodents, containing 344 chemical compounds with 19 discrete labels that indicate carcinogenicity for male and female rats. **PROTEINS** (Borgwardt et al. 2005) aims to classify proteins into enzyme and non-enzyme structures. Nodes represent secondary structure elements (SSEs) connected by edges if they are neighbors in the amino-acid sequence or in 3D space. There are three discrete labels: sheet, helix, and turn structures. As for social network datasets, **IMDB-B** & **IMDB-M** (Yanardag and Vishwanathan 2015) are movie collaboration datasets consisting of actors’ and actresses’ ego-networks from IMDB. Nodes represent actors/actresses, and edges connect them if they appear in the same movie. Each graph originates from a specific movie genre and the task is to classify their genre. The primary difference between the two datasets lies in the number of categories: IMDB-B has two (Action and Romance), while IMDB-M includes three (Comedy, Romance, and Sci-Fi). Table 11 provides the statistics of the graph classification datasets em-

ployed in this study.

## I Supplementary experimental settings

The well-known small-world effect (Milgram 1967) in network science informs that even large-scale networks possess a finite diameter, implying that the neighbor scope under consideration (denoted by  $K$ ) need not be excessively large, typically around 6. In all our experiments, we set  $K = 10$ , a value considerably larger than the average network diameter.

**Node classification.** We train the proposed HiGCN model with the learning rate  $lr \in \{0.01, 0.05, 0.1, 0.2, 0.3\}$  and the weight decay  $wd \in \{0.0, 0.0001, 0.001, 0.005, 0.1\}$ . We leverage Adam as the model optimizer and establish the maximum number of epochs at 1000 for all datasets. We utilize 2 linear layers with 32 hidden units for the NN component. The activation function is log Softmax, and the loss function is negative log Likelihood loss (NLL loss). We employ RayTune to randomly select hyperparameters with the goal of optimizing the accuracy score on the validation set.

**Simplicial data imputation.** We use a two-layer (MLP) with 32 hidden units for the NN component. We adopt the  $\ell_1$  norm to train the NNs over known signals for 500 iter-

SCs	$n$	$n_1$	$n_2$	$n_3$	$n_4$	$n_5$
DBLP	41910	23334	10951	6279	4684	3756
Geology	52259	52373	50051	62869	98846	159879
History	29354	5554	9334	24428	65770	166285

Table 10: Statistics of coauthorship complexes.

Dataset	Graphs	Classes	$\langle n \rangle$	$\langle n_1 \rangle$	$\langle n_2 \rangle$	$\langle k \rangle$
MUTAG	188	2	17.93	19.79	0.00	2.21
PTC	344	2	25.56	25.96	0.04	2.03
PROTEINS	1113	2	39.06	72.82	27.40	3.73
IMDB-B	1000	2	19.77	96.53	391.99	9.77
IMDB-M	1500	3	13.00	65.94	305.90	10.14

Table 11: Statistics of graph classification datasets.

ations using the Adam optimizer with a learning rate  $lr \in \{0.001, 0.005, 0.01, 0.05\}$ ,  $\alpha \in \{0.1, 0.3, 0.5, 0.7, 0.9\}$  and weight decay  $wd = 0$ . Each experiment is performed for 10 different random weight initializations. We run a grid search to select hyperparameters with the goal of optimizing the Kendall correlation for the entire signal.

**Graph classification.** We set the parameter  $P = 2$  in this experiment, implying that the highest order of the simplices under consideration is 2-simplices, i.e., each graph is lifted to a clique 2-complex, where 0-simplices are initialized with the original node signals as prescribed in (Xu et al. 2019). Our training process starts from an initial learning rate, which decayed after a fixed amount of epochs. We implement readout operations by conducting averaging or summation depending on the dataset to calculate feature vectors derived from the hidden states. Although we do not deploy any sophisticated simplicial complex pooling operator within this study, we anticipate that this concept presents a compelling trajectory for future research endeavors. We run a grid search to tune batch size among  $\{32, 64\}$ , hidden dimension among  $\{32, 64\}$ , dropout rate among  $\{0.0, 0.3\}$ , initial learning rate among  $\{0.0005, 0.001, 0.005, 0.01\}$ . We follow the same evaluation protocol of (Xu et al. 2019), conducting a 10-fold cross-validation procedure and reporting the maximum average validation accuracy across folds.

**Baselines.** For the baseline methods BernNet (He et al. 2021), GGCN (Yan et al. 2021), APPNP (Gasteiger, Bojchevski, and Günnemann 2019), GPRGNN (Chien et al. 2020), GIN (Xu et al. 2019), SNN (Ebli, Defferrard, and Spreemann 2020), SGAT (Lee, Ji, and Tay 2022) and MPSN (Bodnar et al. 2021), we directly use the code provided by the authors. For the remaining methods, we use the Pytorch Geometric library (Fey and Lenssen 2019) for implementations. We adopt the best hyperparameters provided by the authors if available; otherwise, hyperparameters are searched within the same hyperparameter space as our model. The hyperparameters adopted can be found in our code.

**Computing infrastructure.** We utilize NetworkX, Pytorch, and Pytorch Geometric for model construction. All experiments are conducted on two Nvidia GeForce RTX 3060 GPUs with 64 GB memory.